Code No.	N1	N2-1	N2-2	N3	N4	N5	N6-1	N6-2	N6-3	N7	N8	N9-1
GU; ODS (Amid)	5.0 (8.8)	5.3 (7.9)	5.3 (9.5)	6.0 (7.8)	6.2 (7.0)	7.3 (6.0)	7.6 (4.2)	7.6 (5.0)	7.6 (4.6)	7.9 (3.3)	8.1 (7.3)	8.2 (5.6)
Mass (Da)	1800	1638	1962	1638	1475	1313	989	1151	1192	827	1679	1354
Structure	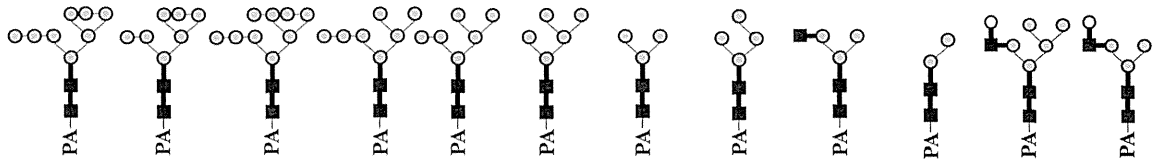											

N9-2	N9-3	N10	N11-1	N11-2	N11-3	N12	N13	N14	N15	N16	N17
8.2 (6.4)	8.3 (8.2)	9.3 (5.0)	10.5 (3.7)	10.5 (4.6)	10.5 (6.9)	11.2 (6.1)	12.8 (5.3)	13.0 (5.0)	13.3 (6.2)	13.5 (6.3)	14.2 (7.3)
1516	1841	1395	973	1135	1720	1500	1541	1338	1704	1704	1866
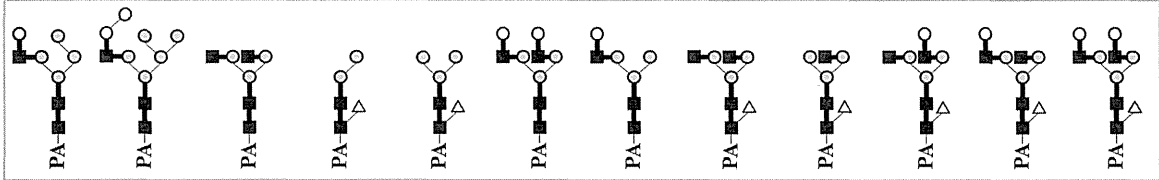											

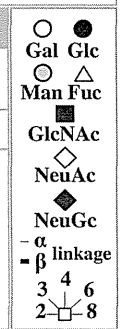

M1	M2-1	M2-2	M2-3	M3	M4	M5	M6-1	M6-2	M7	M8	M9	M10	M11-1	M11-2
7.6 (7.5)	7.9 (5.8)	7.9 (6.6)	7.9 (7.5)	8.1 (7.5)	8.4 (6.7)	8.6 (7.0)	9.0 (5.3)	9.0 (6.1)	10.1 (7.1)	10.3 (7.9)	10.6 (7.1)	11.0 (6.3)	11.3 (6.6)	11.3 (8.8)
1970	1646	1808	2027	1986	1824	1970	1646	1808	2011	2173	2027	1792	2011	2360
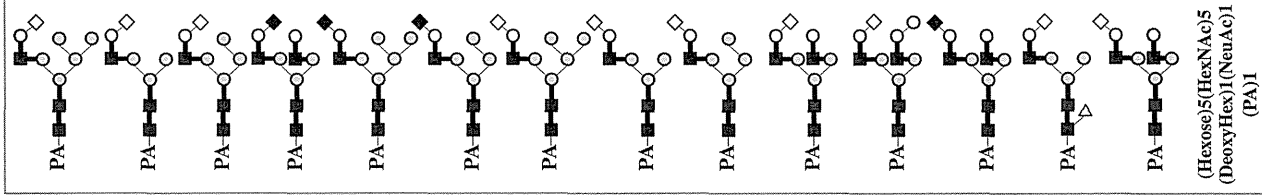														

M12	M13	M14-1	M14-2	M15	M16	M17	M18	M19	M20-1	M20-2	M21	M22	M23
11.5 (7.4)	11.3 (7.4)	11.8 (6.5)	11.8 (5.6)	12.1 (8.3)	13.3 (7.5)	13.7 (8.3)	13.8 (7.4)	14.0 (8.2)	14.2 (7.5)	14.2 (8.2)	14.5 (8.3)	15.1 (6.9)	15.3 (7.8)
2173	2116	1954	1792	2173	2157	2320	2360	2522	2173	2522	2344	2157	2320
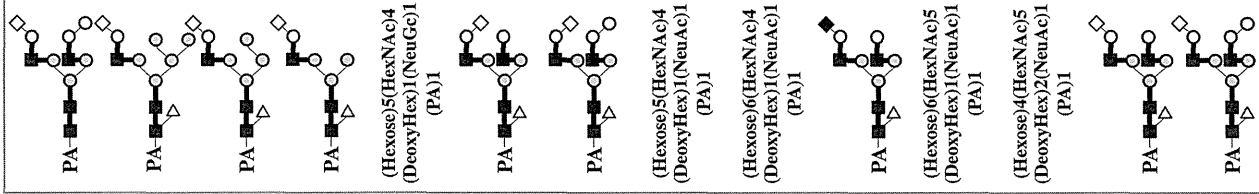													

D1	D2	D3	D4-1	D4-2	D5-1	D5-2	D6	D7	D8	D9	D10-1	D10-2	D11	D12
7.0 (8.2)	8.3 (7.8)	9.3 (8.6)	10.6 (6.9)	10.6 (7.3)	10.9 (7.4)	10.9 (8.1)	12.1 (6.4)	13.5 (7.7)	13.9 (6.8)	14.1 (7.5)	14.2 (7.2)	14.2 (7.7)	15.0 (7.2)	15.9 (6.7)
2334	2334	2480	2302	2302	2334	2480	2302	2448	2537	2854	2448	2480	2464	2448
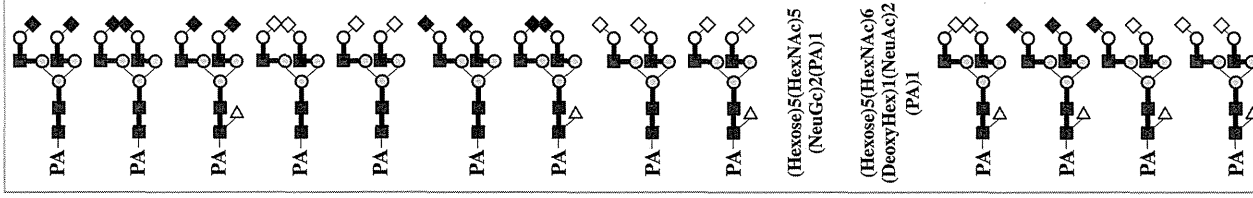														

Figure 8. Structures of neutral, monosialyl, and disialyl PA-oligosaccharides in iPSCs, iPSC-CM, and heart cells. Glucose units (GU) were calculated from the peak elution times for the ODS column in Figure 5, 6 and 7, and the amide column (data not shown). Average mass (Mass) calculated from the *m/z* values of $[M+Na]^+$ or $[M+H]^+$ ion for neutral, $[M-H]^-$ ion for monosialyl, and $[M-H]^-$ & $[M+Na-2H]^-$ ions for disialyl PA-oligosaccharides.
doi:10.1371/journal.pone.0111064.g008

iPSC-CMs (959A2-1 CM: 77.4%, 959C1-1 CM: 60.0% and 956F-1 CM: 65.1%), and lowest in the Heart (46.9%). The quantity of monofucosylated, difucosylated, and other types of *N*-glycans were greater in the iPSC-CMs and Heart (Figure 8, 9).

Sialyl *N*-glycans increased with cardiomyogenic differentiation

The quantity of monosialyl *N*-glycans (MS) calculated from the total volume of M1–M23 increased in iPSC-CMs (959A2-1 CM: 6.4%, 959C1-1 CM: 15.7% and 956F-1 CM: 10.5%) and Heart (19%) and were low in iPSCs (959A2-1: 0.5%, 959C1-1: 0.7% and 956F-1: 1.1%). The disialyl *N*-glycans (DS; D1–D12) yielded a similar pattern. The quantity of asialyl *N*-glycans (AS; N1–N17) decreased in iPSC-CMs (959A2-1 CM: 89.2%, 959C1-1 CM: 79.4% and 956F-1 CM: 81.7%) and Heart (55.3%) in comparison to the iPSCs (959A2-1: 96.9%, 959C1-1: 98.1% and 956F-1: 95.8%) (Figure 9, 10).

Rarely expressed *N*-glycans

The sialic acids identified in this study were either *N*-acetyl neuraminic acid (NeuAc) or *N*-glycolyl neuraminic acid (NeuGc). The quantity of monosialyl and disialyl *N*-glycans containing only NeuAc (A, A/A) was lowest in iPSCs (959A2-1: 2.5%, 959C1-1: 1.7% and 956F-1: 3.7%) and similar in iPSC-CMs (959A2-1 CM: 10.6%, 959C1-1 CM: 21% and 956F-1 CM: 18%) and the Heart (8%). The quantity of monosialyl and disialyl *N*-glycans containing only NeuGc (G, G/G) was markedly higher in the Heart (32.8%) than in iPSCs (959A2-1: 0.6%, 959C1-1: 0.1% and 956F-1: 0.5%) or iPSC-CMs (959A2-1 CM: 0%, 959C1-1 CM: 0% and 956F-1 CM: 0%) (Figure 10a).

Expression of glycosyl transferase, ST3Gal-III, ST3Gal-IV, ST6Gal-I, and CMAH in the iPSCs, iPSC-CMs, and Heart was assessed by RT-PCR to explore the glycan structures responsible for the differences between groups. The Heart expressed high levels of CMAH (0.91 ± 0.13/GAPDH); levels in the iPSCs and iPSC-CMs were markedly lower (iPSCs: 959A2-1 0.011 ± 0.0065/GAPDH, 959C1-1 0.013 ± 0.0070/GAPDH, 956F-1 0.0045 ± 0.0042/GAPDH, $P<0.05$; iPSC-CM: 959A2-1 CM 0.21 ± 0.16/GAPDH, 959C1-1 CM 0.19 ± 0.04, 956F-1 CM 0.45 ± 0.31, $P<0.05$). Expression of ST3Gal-III was significantly higher in the Heart (0.98 ± 0.13/GAPDH) than in iPSCs (959A2-1: 0.21 ± 0.05/GAPDH, 959C1-1: 0.18 ± 0.07/GAPDH, 956F-1: 0.27 ± 0.05/GAPDH) and iPSC-CMs (959A2-1 CM: 0.40 ± 0.10/GAPDH, 959C1-1 CM: 0.35 ± 0.09/GAPDH, 956F-1 CM: 0.66 ± 0.18); expression of ST3Gal-IV did not differ between groups. ST6Gal-I expression was significantly higher in iPSC-CMs (959A2-1 CM: 1.87 ± 0.41/GAPDH, 959C1-1 CM: 1.95 ± 0.22/GAPDH, 956F-1 CM: 3.08 ± 1.27/GAPDH) than in iPSCs (959A2-1: 0.51 ± 0.18/GAPDH, 959C1-1: 0.40 ± 0.09/GAPDH, 956F-1: 0.62 ± 0.29/GAPDH) and the Heart (1.04 ± 0.13/GAPDH) (Figure 10b).

Discussion

Sixty-eight different *N*-glycans were isolated from iPSCs, iPSC-CMs, and the Heart. The structures of 60 *N*-glycans were identified, based on their HPLC elution peaks (Figure 8, Table S1-S5). Each preparation contained a combination of neutral, monosialyl, and disialyl *N*-glycans.

The molar ratios of high-mannose, monofucosylated, and difucosylated *N*-glycans were substantially different between groups (Figure 9), although no clear differences in the abundance of these glycans were found. The decrease in high-mannose *N*-glycans and increase of fucosylated *N*-glycans in iPSC-CMs versus iPSCs is consistent with a previous report on a comparison of ESC derived cardiomyocytes to undifferentiated ESCs [18]. Generally, all *N*-glycans are synthesized from the high-mannose type by a large array of sequentially and competitively acting biosynthetic enzymes located throughout the endoplasmic reticulum and Golgi apparatus [26], indicating that the high-mannose type of *N*-glycans could be categorized as a marker of immaturity. In this study, the high-mannose *N*-glycans were highest in the immature iPSC and lowest in the Heart, or mature tissue; thus, the quantity of high-mannose-type *N*-glycans might be an indicator of maturity in iPSC-derivatives and the iPSC-CMs in our protocol may still be immature in comparison to cardiac tissue.

Clear differences in glycan abundance were observed, such as hybrid and complex types represented by N9-1, N9-3, N15, N16, M1, M2-1, M2-2, M7, M8, M10, M12, M13, M14-1, M14-2, M17, M18, M20-2, D6 and D9 in iPSC-CMs, M2-3, M3, M4, M9, M11-1, M11-2, M20-1, M21, D1, D2, D3, D5-1, D5-2, D10-2 and D11 in Heart and N14 and M15 in iPSCs; these may also be indicators of maturation stage. In addition, expression of monosialyl and disialyl *N*-glycans in iPSC-CMs fell between the levels observed in the iPSCs and Heart, as were the molar ratios, indicating that the iPSC-CMs may still be immature stage. While many *N*-glycolyl neuraminic acid (NeuGc) structures were detected in the Heart, iPSCs and iPSC-CMs did not contain NeuGc in their sialyl structures, except for D8. Moreover, the molar ratio of NeuAc was low in iPSCs and iPSC-CMs. This finding is one of the clearest differences between iPSCs or iPSC-CMs and Heart cells.

The proposed spectra-based composition of the D8 glycans in iPSCs was [(Hexose)5(HexNAc)5(NeuGc)2(PA)1], indicating that it contains NeuGc. However, D8 might be quite a rare exception because transcript levels of CMAH, which catalyzes the conversion of NeuAc to NeuGc, was quite low in iPSCs in comparison to the Heart. This data suggests that during the process of reprograming, iPSCs suppress or eliminate CMAH activity. We conclude that iPSCs contain less sialic acid (especially NeuGc) and high-mannose structures are abundant in the *N*-glycans. In contrast, heart cells produce numerous sialyl-*N*-glycans, especially NeuGc. Transcript levels of CMAH tended to increase in iPSC-CMs relative to iPSCs, suggesting cardiomyogenic differentiation may induce expression of CMAH. If the iPSC-CMs could be matured more closely to the Heart by some additional methods of culture, the quantity of high mannose type of *N*-glycans might decrease more closely to the Heart, and might produce *N*-glycans containing NeuGc, followed by the expression of CMAH.

A terminal NeuGc, the Hanganutziu-Deicher (H-D) epitope [27], is widely distributed in the animal kingdom with the exception of humans and chickens. Expression of NeuGc is controlled by CMAH activity. Irie et al. [28] and Chou et al. [29] cloned the cDNA for human CMAH and reported that the *N*-terminal truncation of human CMAH is caused by deletion of Exon 6, a 92-base pair segment in the genomic DNA. Expression of this truncation in the heart eliminates NeuGc in sialyl

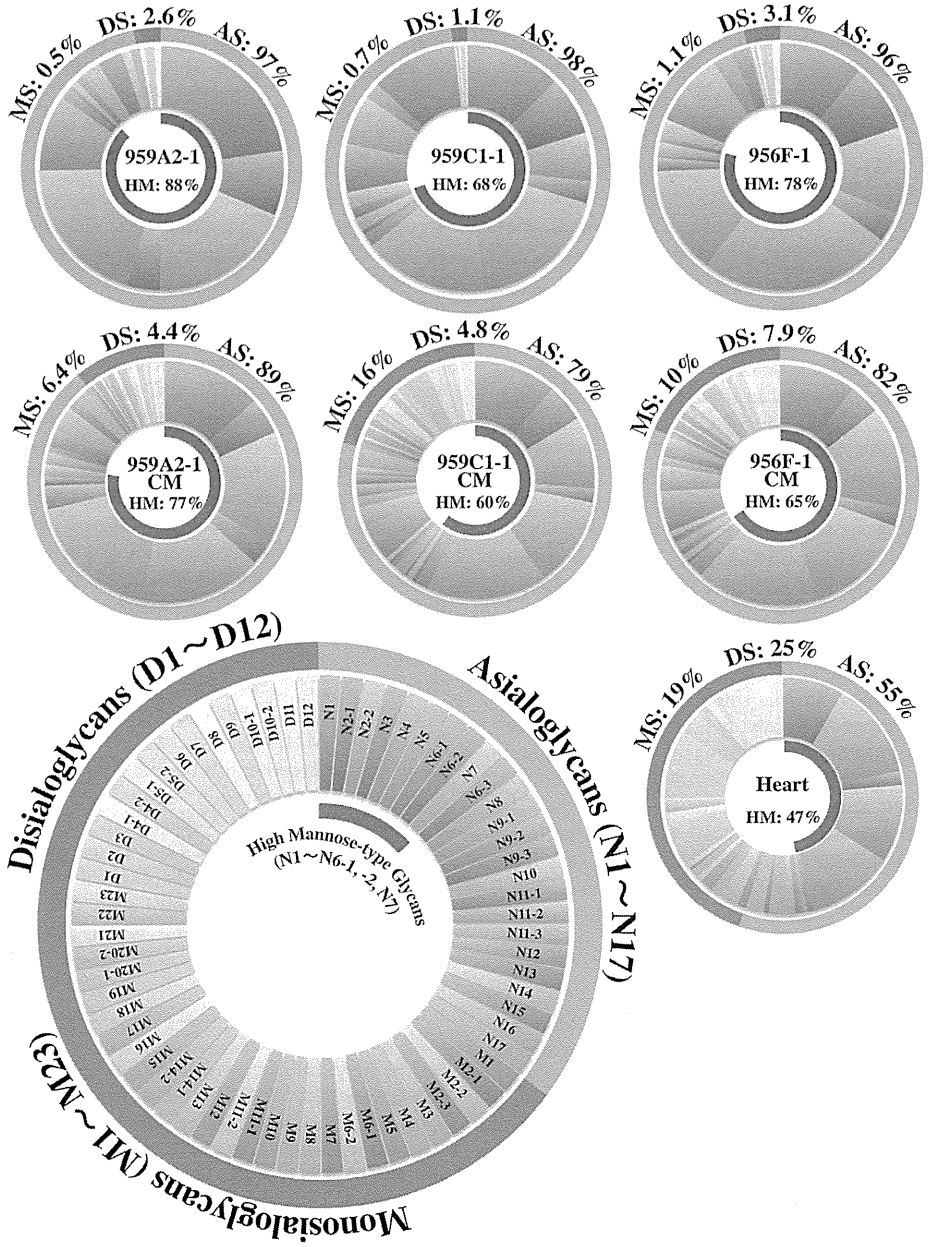

Figure 9. Relative quantities of neutral, monosialyl, and disialyl PA-oligosaccharides in iPSCs, iPSC-CM, and heart cells. Relative quantities of each glycan, calculated from the peak area in Figure 5, 6 and 7 vs. total *N*-glycan content in each cell, were expressed in the doughnut charts. Relative quantities of the asialoglycans, the monosialoglycans and the disialoglycans were showed outside of the charts, and relative quantities of the high mannose type glycans were showed inside of the charts. Asialoglycan (AS): the total volume of N1-N17; Monosialoglycan (MS): the total volume of M1-M23; Disialoglycan (DS): the total volume of D1-D12, High mannose-type glycan (HM): the total volume of N1–N6-1, N6-2, N7.
doi:10.1371/journal.pone.0111064.g009

structures. If human iPSCs or iPSC-CMs do not express CMAH in the same way as murine iPSCs or iPSC-CMs, there may be no difference between human iPSCs, iPSC-CMs, and the human Heart. Further study on human iPSC-CM will be needed to completely understand the features of the sialyl acid of *N*-glycans.

It was reported that human iPSCs produced α2,6sialyl glycans but did not contain α2,3sialyl structures, in contrast to human fibroblast, the origin of iPSCs, which produced α2,3sialyl but not α2,6sialyl structures [30,31]. The murine iPSCs in this study contained α2,3sialyl structures in NeuAc, M5, M23, D4-1, D10-1 and D12, and the iPSC-CMs produced α2,3 and α2,6sialyl structures in NeuAc. These differences may be due to variations between species, because mouse Heart cells also contained α2,3 and α2,6sialyl structures in NeuGc. Further studies are needed to characterize the glycome shift in the production and differentiation of iPSCs.

Type I Lactose structures were not detected, although over 98% of glycans in each cell were accounted for in this study. The *N*-glycans of N9-3, M8, M12, M17, and M23, which were identified after α-galactosidase digestion, contained Galα1-6Gal, not only in

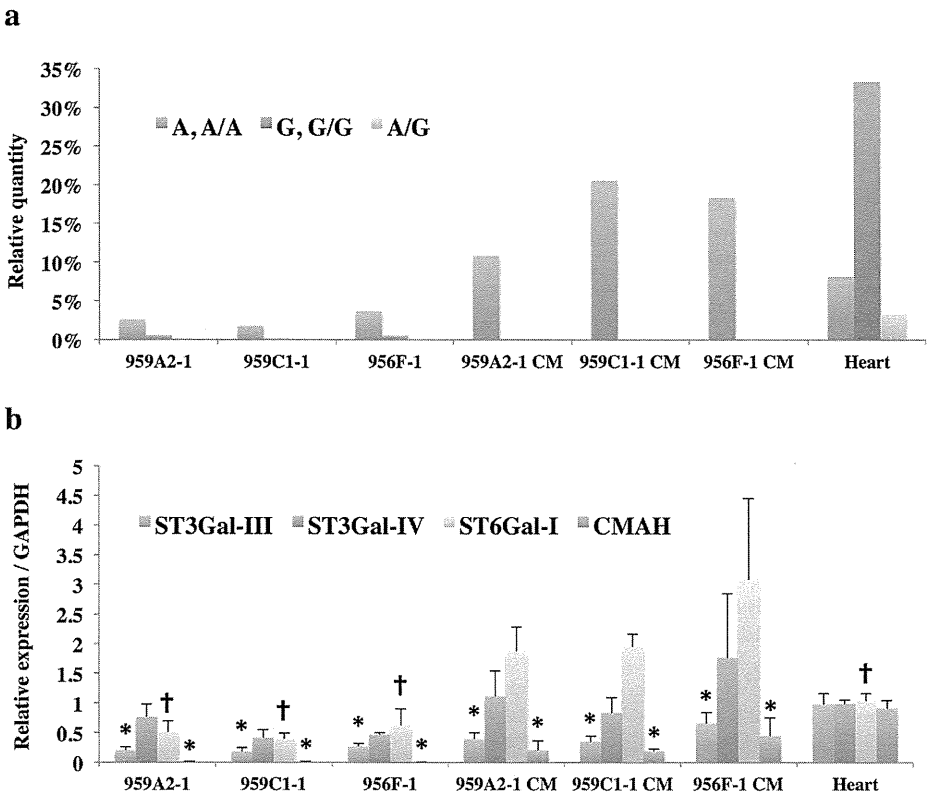

Figure 10. Rarely expressed NeuGc-containing glycans in iPSCs and iPSC-CMs. (a) Relative quantities of NeuAc- and NeuGc-containing glycans; Monosialoglycans containing NeuAc and Disialoglycans containing two NeuAc (A, A/A): the total volume of M1, M2-1, M2-2, M5-M8, M10-M14, M16-M19, M20-2, M21-M23, D4-1, D4-2, D6, D7, D9, D10-1, D12, Disialoglycan containing NeuAc and NeuGc (A/G): D11, Monosialoglycan containing NeuGc and Disialoglycan containing two NeuGc (G, G/G): the total volume of M2-3, M3, M4, M9, M15, M20-1, D1-D3, D5-1, D5-2, D8, D10-2. (b) Transcript expression of ST3Gal-III, ST3Gal-IV, ST6Gal-I, and CMAH; Transcript expression of glycosyltransferases in iPSCs, iPSC-CM, and heart cells was analyzed by real-time PCR. Results are expressed as the mean ± standard deviation. *P<0.05 vs. Heart, †P<0.05 vs. iPSC-CM (all of the 959A2-1 CM, 959C1-1 CM and 956F-1 CM).
doi:10.1371/journal.pone.0111064.g010

the neutral glycans but also in the monosialyl *N*-glycans of the iPSC-CM preparation. The same structure was not found in iPSCs, but only one structure, M23, was present in Heart cells. Therefore, in iPSC-CMs, Galα1-6Gal enzyme activity appears to be up-regulated in comparison to wild-type myocardium, although enzyme activity was not assessed by RT-PCR because of the limited availability of genetic sequence data.

The D8 was identified in all of three iPSC lines and not in the iPSC-CMs and Heart. This structure, unfortunately not identified in this study, may be useful as markers of undifferentiated iPSCs in the same way as well-known pluripotency biomarkers such as stage-specific embryonic antigens (SSEA)-3, SSEA-4 (glycosphingolipids) [32].

Previous MALDI-TOF/MS and MS/MS studies concluded that many kinds of *N*-glycans are found in organs and cells. The number of detected *N*-glycans is attributed to the sensitivity of the MS and HPLC methods employed. That is, MS data are sensitive and can be rapidly obtained, but a glycan structure is identified based only on the calculated molecular weight. Therefore, discriminating between isomeric structures is difficult. On the other hand, it thus appears that the accuracy of the data presented here using HPLC mapping in conjunction with a MALDI-TOF technique provides much more detailed information. Our data were used to identify the representative features of each *N*-glycan in these three cell types.

There may be a concern that the heart tissue used in this study contains connective tissues, vessels or nerves other than cardiomyocytes. Therefore, some of the *N*-glycans detected from the Heart sample might be derived from the tissues other than cardiomyocytes. However, heart is majority composed by cardiomyocytes, and furthermore, even if a small amount of *N*-glycans derived from connective tissues were contaminated in the Heart sample, the main evidences in this study, such as the proportion of the high-mannose type *N*-glycans, the ratio of the active sialyltransferase genes, the existence of NeuGc, and the uncommonness of Galα1-6 Gal, are essentially not affected.

In summary, murine iPSCs were rich in high-mannose type *N*-glycans but very poor in sialyl type *N*-glycans. Murine heart tissue contained a relatively low volume of high-mannose glycans, but was very rich in neuraminic acid, especially NeuGc type sialyl structures. Under these conditions, the volume of each type of glycan was similar for iPSC-CMs and iPSCs. That is, they were rich in high-mannose and relatively poor in sialyl type *N*-glycans by volume. In addition, most of the sialyl structures of the iPSC-CMs were different from those of the Heart, and the iPSC-CMs expressed no NeuGc. Moreover, the iPSC-CMs produced several unique glycans with the Galα1-6Gal structure. These results

provide important data that can be useful in future clinical iPSC studies.

It is quite important to investigate the meaning of *N*-glycans transitions during the cardiomyogenic differentiation presented in this study, for deeply understanding the relationship between the *N*-glycan expression and cardiomyogenic differentiation. Knock-out or knock-down of the genes related to cardiomyogenic differentiation or glycosylation may be useful for such purpose. However, the *N*-glycan signature in the cell surface is determined by a variety of the genes. Knock-out or knock-down of a single gene related to cardiomyogenic differentiation would alter an array of gene expressions, such as sarcomere proteins, transcriptional factors, or cell surface proteins, all of which would affect the signature of *N*-glycans in the cell surface. Therefore, the data interpretation for relationship between expression of a single gene and *N*-glycan signature would be difficult. Some different experimental approach may be needed to investigate the meaning of change in *N*-glycan expression during cardiomyogenic differentiation.

Supporting Information

Table S1 Structures and relative quantities of neutral (Table S1, S2) PA-oligosaccharides derived from iPSC, iPSC-CM, and heart cells. a. Glucose units (GU) were calculated from the peak elution times of the peaks obtained from the ODS column in Figure 5, 6, 7 and the Amide column (data not shown). b. Average mass calculated from the *mlz* values of $[M+Na]^+$ or $[M+H]^+$ ion for neutral, $[M-H]^-$ ion for mono-sialyl, and $[M-H]^-$ & $[M+Na-2H]^-$ ions for di-sialyl PA-oligosaccharides. c. PA-oligosaccharide structures. d. mol% was calculated from the peak area versus total *N*-glycan content in each cell
(TIFF)

Table S2 Structures and relative quantities of neutral (Table S1, S2) PA-oligosaccharides derived from iPSC, iPSC-CM, and heart cells.
(TIFF)

Table S3 Structures and relative quantities of mono-sialyl (Table S3, S4) PA-oligosaccharides derived from iPSC, iPSC-CM, and heart cells.
(TIFF)

Table S4 Structures and relative quantities of mono-sialyl (Table S3, S4) PA-oligosaccharides derived from iPSC, iPSC-CM, and heart cells.
(TIFF)

Table S5 Structures and relative quantities of disialyl PA-oligosaccharides derived from iPSC, iPSC-CM, and heart cells.
(TIFF)

Video S1
(MP4)

Acknowledgments

Our deepest appreciation goes to Professor Shinya Yamanaka and Keisuke Okita of the Center for iPS Cell Research and Application, Kyoto University, who kindly provided the murine iPSCs. We also thank Sachiko Kondo and Uichiro Yabe of MBL, Nagoya, Japan, who gave invaluable comments regarding *N*-glycan analysis.

Author Contributions

Conceived and designed the experiments: TK S. Miyagawa S. Miyagawa JL YS. Performed the experiments: TK AY NK AK EI AM HE KT. Analyzed the data: TK S. Miyagawa YS. Contributed reagents/materials/analysis tools: TK AY JL. Wrote the paper: TK S. Miyagawa YS SF. Obtained permission for use of cell line: S. Miyagawa AS YS.

References

1. Gonzales C, Pedrazzini T (2009) Progenitor cell therapy for heart disease. Exp Cell Res 315: 3077–3085.
2. Shah AM, Mann DL (2011) In search of new therapeutic targets and strategies for heart failure: recent advances in basic science. Lancet 378: 704–712.
3. Yoshida Y, Yamanaka S (2010) Recent stem cell advances: induced pluripotent stem cells for disease modeling and stem cell-based regeneration. Circulation 122: 80–87.
4. Yoshida Y, Yamanaka S (2011) iPS cells: A source of cardiac regeneration. Journal of Molecular and Cellular Cardiology 50: 327–332.
5. Kawamura M, Miyagawa S, Miki K, Saito A, Fukushima S, et al. (2012) Feasibility, safety, and therapeutic efficacy of human induced pluripotent stem cell-derived cardiomyocyte sheets in a porcine ischemic cardiomyopathy model. Circulation 126: S29–37.
6. Mercola M, Colas A, Willems E (2013) Induced pluripotent stem cells in cardiovascular drug discovery. Circ Res 112: 534–548.
7. Sinnecker D, Goedel A, Laugwitz KL, Moretti A (2013) Induced pluripotent stem cell-derived cardiomyocytes: a versatile tool for arrhythmia research. Circ Res 112: 961–968.
8. Kamakura T, Makiyama T, Sasaki K, Yoshida Y, Wuriyanghai Y, et al. (2013) Ultrastructural maturation of human-induced pluripotent stem cell-derived cardiomyocytes in a long-term culture. Circ J 77: 1307–1314.
9. Kuzmenkin A, Liang H, Xu G, Pfannkuche K, Eichhorn H, et al. (2009) Functional characterization of cardiomyocytes derived from murine induced pluripotent stem cells in vitro. FASEB J 23: 4168–4180.
10. Varki A (1993) Biological roles of oligosaccharides: all of the theories are correct. Glycobiology 3: 97–130.
11. Haltiwanger RS, Lowe JB (2004) Role of glycosylation in development. Annu Rev Biochem 73: 491–537.
12. Ohtsubo K, Marth JD (2006) Glycosylation in cellular mechanisms of health and disease. Cell 126: 855–867.
13. Surani MA (1979) Glycoprotein synthesis and inhibition of glycosylation by tunicamycin in preimplantation mouse embryos: compaction and trophoblast adhesion. Cell 18: 217–227.
14. Akama TO, Nakagawa H, Sugihara K, Narisawa S, Ohyama C, et al. (2002) Germ cell survival through carbohydrate-mediated interaction with Sertoli cells. Science 295: 124–127.
15. Hato M, Nakagawa H, Kurogochi M, Akama TO, Marth JD, et al. (2006) Unusual N-glycan structures in alpha-mannosidase II/IIx double null embryos identified by a systematic glycomics approach based on two-dimensional LC mapping and matrix-dependent selective fragmentation method in MALDI-TOF/TOF mass spectrometry. Mol Cell Proteomics 5: 2146–2157.
16. Lau KS, Partridge EA, Grigorian A, Silvescu CI, Reinhold VN, et al. (2007) Complex N-glycan number and degree of branching cooperate to regulate cell proliferation and differentiation. Cell 129: 123–134.
17. Kraushaar DC, Rai S, Condac E, Nairn A, Zhang S, et al. (2012) Heparan sulfate facilitates FGF and BMP signaling to drive mesoderm differentiation of mouse embryonic stem cells. J Biol Chem 287: 22691–22700.
18. Amano M, Yamaguchi M, Takegawa Y, Yamashita T, Terashima M, et al. (2010) Threshold in stage-specific embryonic glycotypes uncovered by a full portrait of dynamic N-glycan expression during cell differentiation. Mol Cell Proteomics 9: 523–537.
19. Okita K, Nakagawa M, Hyenjong H, Ichisaka T, Yamanaka S (2008) Generation of mouse induced pluripotent stem cells without viral vectors. Science 322: 949–953.
20. Miki K, Uenaka H, Saito A, Miyagawa S, Sakaguchi T, et al. (2012) Bioengineered myocardium derived from induced pluripotent stem cells improves cardiac function and attenuates cardiac remodeling following chronic myocardial infarction in rats. Stem Cells Transl Med 1: 430–437.
21. Yu T, Miyagawa S, Miki K, Saito A, Fukushima S, et al. (2013) In vivo differentiation of induced pluripotent stem cell-derived cardiomyocytes. Circ J 77: 1297–1306.
22. Tohyama S, Hattori F, Sano M, Hishiki T, Nagahata Y, et al. (2013) Distinct metabolic flow enables large-scale purification of mouse and human pluripotent stem cell-derived cardiomyocytes. Cell Stem Cell 12: 127–137.
23. Takahashi N, Khoo KH, Suzuki N, Johnson JR, Lee YC (2001) N-glycan structures from the major glycoproteins of pigeon egg white: predominance of terminal Galalpha(1)Gal. J Biol Chem 276: 23230–23239.

24. Takahashi N, Kato K (2003) GALAXY(Glycoanalysis by the Three Axes of MS and Chromatography): a Web Application that Assists Structural Analyses of N-Glycans. Trends in Glycoscience and Glycotechnology 15 No.84: 235–251.
25. Yagi H, Takahashi N, Yamaguchi Y, Kimura N, Uchimura K, et al. (2005) Development of structural analysis of sulfated N-glycans by multidimensional high performance liquid chromatography mapping methods. Glycobiology 15: 1051–1060.
26. Dalziel M, Crispin M, Scanlan CN, Zitzmann N, Dwek RA (2014) Emerging principles for the therapeutic exploitation of glycosylation. Science 343: 1235681.
27. Varki A (2009) Multiple changes in sialic acid biology during human evolution. Glycoconj J 26: 231–245.
28. Irie A, Koyama S, Kozutsumi Y, Kawasaki T, Suzuki A (1998) The molecular basis for the absence of N-glycolylneuraminic acid in humans. J Biol Chem 273: 15866–15871.
29. Chou HH, Takematsu H, Diaz S, Iber J, Nickerson E, et al. (1998) A mutation in human CMP-sialic acid hydroxylase occurred after the Homo-Pan divergence. Proc Natl Acad Sci U S A 95: 11751–11756.
30. Hasehira K, Tateno H, Onuma Y, Ito Y, Asashima M, et al. (2012) Structural and quantitative evidence for dynamic glycome shift on production of induced pluripotent stem cells. Mol Cell Proteomics 11: 1913–1923.
31. Tateno H, Toyota M, Saito S, Onuma Y, Ito Y, et al. (2011) Glycome diagnosis of human induced pluripotent stem cells using lectin microarray. J Biol Chem 286: 20345–20353.
32. Fujitani N, Furukawa J, Araki K, Fujioka T, Takegawa Y, et al. (2013) Total cellular glycomics allows characterizing cells and streamlining the discovery process for cellular biomarkers. Proc Natl Acad Sci U S A 110: 2105–2110.

Effect of Intermittent Administration of Teriparatide (Parathyroid Hormone 1-34) on Bone Morphogenetic Protein-Induced Bone Formation in a Rat Model of Spinal Fusion

Tokimitsu Morimoto, MD, Takashi Kaito, MD, PhD, Masafumi Kashii, MD, PhD, Yohei Matsuo, MD, Tsuyoshi Sugiura, MD, Motoki Iwasaki, MD, and Hideki Yoshikawa, MD, PhD

Investigation performed at the Departments of Orthopedic Surgery and Orthopedic Biomaterial Science, Graduate School of Medicine, Osaka University, Osaka, Japan

Background: Although clinical bone morphogenetic protein (BMP) therapy is effective at enhancing bone formation in patients managed with spinal arthrodesis, the required doses are very high. Teriparatide (parathyroid hormone 1-34) is approved by the U.S. Food and Drug Administration to treat osteoporosis and is a potent anabolic agent. In this study, intermittent administration of parathyroid hormone 1-34 combined with transplantation of BMP was performed to elucidate the effect of parathyroid hormone 1-34 on the fusion rate and quality of newly formed bone in a rat model.

Methods: A total of forty-eight male Sprague-Dawley rats underwent posterolateral lumbar spinal arthrodesis with one of three different treatments with recombinant human (rh) BMP-2: (1) 0 μg (control), (2) 2 μg (low dose), or (3) 50 μg (high dose). Each of the rhBMP-2 treatments was studied in combination with intermittent injections of either parathyroid hormone 1-34 (180 μg/kg/wk) or saline solution starting two weeks before the operation and continuing until six weeks after the operation. Osseous fusion was assessed with use of radiographs and a manual palpation test. Microstructural indices of the newly formed bone were evaluated with use of micro-computed tomography. The serum markers of bone metabolism were also quantified.

Results: The fusion rate in the group treated with 2 μg of rhBMP-2 significantly increased (from 57% to 100%) with the administration of parathyroid hormone 1-34 ($p < 0.05$). The fusion rates in the other groups did not change significantly with the administration of parathyroid hormone 1-34. The bone volume density of the newly formed bone significantly increased in both the 2-μg and 50-μg rhBMP-2 treatment groups with the administration of parathyroid hormone 1-34 ($p < 0.01$). Micro-computed tomography scans of the newly formed bone clearly demonstrated an abundance of trabecular bone formation in the group treated with parathyroid hormone 1-34. In addition, serum levels of osteocalcin were significantly increased in the parathyroid hormone 1-34 treatment group.

Conclusions: Intermittent administration of parathyroid hormone 1-34 significantly increased fusion rates in the group treated with low-dose rhBMP-2, and it improved the quality of the newly formed bone in both the high and low-dose groups in a rat model of rhBMP-2-induced spinal fusion.

Clinical Relevance: Our results suggest that the combined administration of rhBMP-2 and parathyroid hormone 1-34 may lead to efficient bone regeneration.

Peer Review: This article was reviewed by the Editor-in-Chief and one Deputy Editor, and it underwent blinded review by two or more outside experts. It was also reviewed by an expert in methodology and statistics. The Deputy Editor reviewed each revision of the article, and it underwent a final review by the Editor-in-Chief prior to publication. Final corrections and clarifications occurred during one or more exchanges between the author(s) and copyeditors.

Disclosure: One or more of the authors received payments or services, either directly or indirectly (i.e., via his or her institution), from a third party in support of an aspect of this work. None of the authors, or their institution(s), have had any financial relationship, in the thirty-six months prior to submission of this work, with any entity in the biomedical arena that could be perceived to influence or have the potential to influence what is written in this work. Also, no author has had any other relationships, or has engaged in any other activities, that could be perceived to influence or have the potential to influence what is written in this work. The complete **Disclosures of Potential Conflicts of Interest** submitted by authors are always provided with the online version of the article.

Autogenous bone-grafting is the current gold standard for achieving spinal fusion. However, its use is limited by the amount of bone available and by the associated donor-site morbidity[1,2]. Moreover, the rate of pseudarthrosis has been reported to range between 5% and 43%[3,4]. These problems have prompted surgeons to identify alternative means for stimulating bone formation.

One possibility is the use of bone morphogenetic proteins (BMPs), which are a group of growth factors belonging to the transforming growth factor superfamily that are known to elicit new bone formation[5-7]. However, the uncontrolled release of high concentrations of BMPs can cause inflammation, soft-tissue edema, and unintended bone formation[8,9]. Thus, the U.S. Food and Drug Administration has approved the use of BMPs in the spine for anterior lumbar spinal arthrodesis only; uses for posterior spinal arthrodesis have been "off label." Therefore, an efficient method for reducing the required dose of BMPs by enhancing the bioactivity is required.

Teriparatide (recombinant human parathyroid hormone [PTH] 1-34) is the only anabolic agent that has been approved by the U.S. Food and Drug Administration for the treatment of osteoporosis[10,11]. Intermittent administration of PTH 1-34 results in osteoblastic proliferation and differentiation, thereby leading to an increase in bone mass[12-14]. Recently, upregulation and modulation of BMP signaling by PTH have been reported[15,16]. These mechanisms indicate the possibility of synergistic bone regeneration by the co-administration of rhBMP-2 and PTH 1-34.

In the present study, intermittent administration of PTH 1-34 combined with BMP transplantation was performed to elucidate the effect of PTH 1-34 on the fusion rate and quality of the newly formed bone in a rat model of spinal fusion.

Materials and Methods

Experimental Design

A total of four dozen eight-week-old male Sprague-Dawley rats (weight, 270 to 290 g) were used. The animals were allocated to one of six different treatment groups by assigning one of three surgical treatments and one of two injection treatments to each rat. Each treatment group consisted of eight animals (see Appendix). The three surgical treatments consisted of (1) implantation of a collagen-only carrier (Groups A and B), (2) implantation of a collagen carrier loaded with 2 μg of rhBMP-2 (Groups C and D), and (3) implantation of a collagen carrier loaded with 50 μg of rhBMP-2 (Groups E and F). The animals in each treatment group were further divided into two subgroups, including rats that also received either (1) injections of PTH 1-34 (Groups B, D, and F) or (2) injections of saline solution (Groups A, C, and E) (see Appendix). rhBMP-2 doses for the low and high-dose groups were based on a preliminary spinal fusion study (data not shown). We chose 2 μg (fusion rate, 50%; concentration, 20 μg/mL) as the low dose because this amount of rhBMP-2 is better suited for elucidating the effect of PTH 1-34 on the fusion rate, and we chose 50 μg (fusion rate, 100%; concentration, 500 μg/mL) as the high dose because this amount of rhBMP-2 reflects the clinical use of high-dose (1500-μg/mL) rhBMP-2.

Injections of PTH 1-34

Rats in the control group were given subcutaneous injections of 0.9% saline solution, whereas rats in the PTH groups were given subcutaneous injections of PTH 1-34 (60 μg/kg) three times a week (total, 180 μg/kg/wk). Injections were initiated two weeks prior to surgery and were continued for six weeks after surgery, at which time the animals were killed.

TABLE I Results of Radiographic Analysis of Spinal Fusion

rhBMP-2 Dosage (μg)	Injected Material* (%)	
	Saline Solution	PTH 1-34
0	0 of 8 (0)	0 of 8 (0)
2	4 of 7 (57)	8 of 8 (100)†
50	7 of 8 (88)	8 of 8 (100)

*The values are given as the number of spines that were found to have successfully fused as assessed with radiographs, with the percentage in parentheses. †At this dosage, the rate of fusion was significantly higher in the group that received PTH 1-34 ($p < 0.05$).

Posterior Spinal Fusion

Preparation of a Collagen Carrier Vehicle

A commercially available absorbable collagen sponge (CollaCote; Integra LifeSciences, Plainsboro, New Jersey) was cut into 5 × 10-mm fragments. Thereafter, the appropriate concentration of rhBMP-2 (0, 2, or 50 μg) was dissolved in phosphate buffered saline solution and applied to the carrier just before implantation.

Surgical Technique of L4-L5 Posterolateral Spinal Arthrodesis

All of the animal procedures were conducted in accordance with the guidelines of the Regulations on Animal Experimentation at Osaka University. The rats were anesthetized with a combination of 0.15 mg/kg of medetomidine (Domitor; Nippon Zenyaku Kogyo, Fukushima, Japan), 2 mg/kg of midazolam (Dormicum; Astellas Pharma, Tokyo, Japan), and 2.5 mg/kg of butorphanol (Vetorphale; Meiji Seika, Tokyo, Japan). As per the usual method[16,17], a posterior midline skin incision was made, followed by two separate paramedian incisions in the lumbar fascia 3 mm from the midline, through which the transverse processes were exposed. The L4 and L5 transverse processes were decorticated with use of a high-speed burr. Subsequently, a collagen sponge containing 0, 2, or 50 μg of rhBMP-2 was implanted on each side. The rats were housed in separate cages and allowed to eat and drink ad libitum while their condition was monitored daily.

Euthanasia and Analyses

Just prior to euthanization of the animals, blood samples were collected and stored at −80°C until the serum markers of bone metabolism were analyzed. The rats were killed with an overdose of anesthetics at six weeks after surgery. The spinal segments and femora were harvested and fixed with 10% formalin.

Assessment of Fusion

Radiographic Assessment

Fusion between L4 and L5 was evaluated with radiographs made with use of an MX-20 Specimen Radiography System (Faxitron X-Ray, Lincolnshire, Illinois) under consistent conditions (35 kV, 300 μA, 300 seconds). Fusion was considered to have occurred when there was clear evidence of new bone formation and osseous bridging with cortical continuity between the L4 and L5 transverse processes.

Manual Assessment

The explanted lumbar spines were manually tested for intersegmental motion. Any motion detected on either side between the facets or between the transverse processes was considered to be a failure of fusion.

In both assessments, the spines were scored as either fused or not fused independently by three examiners. The L4-L5 segments were considered to be fused only when all three observers agreed.

TABLE II Results of Spinal Fusion as Assessed with Manual Palpation

	Injected Material* (%)	
rhBMP-2 Dosage (μg)	Saline Solution	PTH 1-34
0	0 of 8 (0)	0 of 8 (0)
2	2 of 7 (29)	8 of 8 (100)†
50	8 of 8 (100)	8 of 8 (100)

*The values are given as the number of spines that were found to have successfully fused as assessed with manual palpation, with the percentage in parentheses. †At this dosage, the rate of fusion was significantly higher in the group that received PTH 1-34 ($p < 0.05$).

Micro-Computed Tomography Analysis

Following manual evaluation, the spines were scanned with use of high-resolution micro-computed tomography (micro-CT) (R_mCT; Rigaku Mechatronics, Tokyo, Japan); each sample was scanned twice. The micro-CT data were collected at 90 kV and 200 μA. Visualization and data reconstruction were performed with use of TRI/3D-BON software (RATOC System Engineering, Tokyo, Japan).

Analysis of the Microstructural Indices of the Newly Formed Fusion Mass

The quality of the newly formed fusion mass between the transverse processes where bone did not originally exist was analyzed as described previously[18] (see Appendix). Scanning of the newly formed bone was initiated from the lower end plate level of the L4 vertebral body and continued cranially in 2.0-mm increments (fifty slices) at a resolution of 40 μm per voxel. Bone volume density, trabecular thickness, trabecular number, trabecular separation, thickness of cortical bone, and cortical bone ratio were estimated. The bone volume density corresponds to the ratio of bone volume to fusion-mass volume.

Microstructural Analysis of the Fused Spinal Segments

The tissue volume and bone volume of the total fusion mass were measured (from the bottom to 15 mm cranially from the bottom of the L5 transverse process, for a total of 254 slices) at a resolution of 59 μm per voxel.

Analysis of the Systemic Effects of PTH 1-34

To evaluate the systemic effects of PTH 1-34, the bone volume density of the distal femoral epiphysis and L6 vertebral body was analyzed at a resolution of 40 μm per voxel. Scanning of the distal part of the femur was initiated at 1.5 mm proximal to the growth plate and continued at 3.0-mm increments (for a total of seventy-five slices). Scanning of the L6 vertebral body was initiated at 1.0 mm cranial to the lower growth plate and continued at 3.2-mm increments (for a total of eighty slices).

Analysis of Serum Markers of Bone Metabolism

Serum markers of bone metabolism were analyzed with use of an enzyme-linked immunosorbent assay specific for osteocalcin (Osteocalcin High Sensitive EIA kit [rat]; Takara Bio, Shiga, Japan), type-I collagen cross-linked C-telopeptides (RatLaps ELISA; Immunodiagnostic Systems, Fountain Hills, Arizona), and tartrate-resistant acid phosphatase-5b (RatTRAP Assay; Immunodiagnostic Systems), according to the manufacturer's instructions. Serum from all animals ($n = 47$) was measured once for each marker, with comparisons performed between the groups treated with PTH 1-34 (Groups B, D, and F) and those treated with saline solution (Groups A, C, and E).

Histologic Analysis

The dissected and formalin-fixed spines were demineralized with 50% formic acid and 10% sodium citrate, dehydrated in a graded ethanol series, and

TABLE III Microstructural Indices of Newly Formed Bone

		Injected Material*	
Parameter	rhBMP-2 Dosage (μg)	Saline Solution	PTH 1-34
Tissue volume (mm^3)	2	5.5 ± 5.4	17.1 ± 13.3†
	50	34.8 ± 22.2	29.1 ± 12.0
Bone volume (mm^3)	2	0.7 ± 0.9	3.8 ± 3.2†
	50	2.3 ± 2.7	6.3 ± 2.8†
Bone volume density (%)	2	12.1 ± 5.2	22.1 ± 5.5†
	50	7.1 ± 4.6	22.2 ± 5.5†
Trabecular thickness (μm)	2	142.6 ± 15.1	166.8 ± 31.1‡
	50	153.0 ± 35.9	181.8 ± 17.2†
Trabecular number (mm^{-1})	2	0.8 ± 0.8	0.7 ± 0.2
	50	0.3 ± 0.2	0.6 ± 0.2†
Trabecular separation (μm)	2	305.5 ± 97.2	268.9 ± 56.4
	50	756.9 ± 428.7	298.7 ± 64.9†
Cortical bone ratio (%)	2	41.5 ± 7.6	39.4 ± 11.0
	50	28.8 ± 17.1	30.1 ± 4.8‡
Cortical bone thickness (μm)	2	313.2 ± 77.4	391.3 ± 90.8†
	50	272.4 ± 109.5	365.1 ± 53.0†

*Values are given as the mean and the standard deviation. †At this dosage, the value was significantly higher in the group that received PTH 1-34 ($p < 0.01$). ‡At this dosage, the value was significantly higher in the group that received PTH 1-34 ($p < 0.05$).

embedded in paraffin wax. Serial coronal sections (thickness, 5 μm) of the involved segments were cut and stained with hematoxylin and eosin.

Statistical Analysis

The PASW Statistics computer software program (version 18.0, SPSS, Chicago, Illinois) was used for all of the analyses. The Mann-Whitney U test was used for the comparison of microstructural indices and serum markers of bone metabolism. The chi-square test was used for the comparison of fusion assessments. In all analyses, the level of significance was set at $p < 0.05$.

Source of Funding

This work was supported by a Grant-in-Aid for Scientific Research from the Japan Society for the Promotion of Science (JSPS KAKENHI Grant 25861313).

Results

Spinal Fusion

Radiographic Analysis

One rat in Group C died the day after surgery; thus, a total of forty-seven rats were used for the final analysis. Fusion at L4-L5 in the groups treated with 2 μg of rhBMP-2 significantly increased, from four of seven (57%) to eight of eight (100%), with the administration of PTH 1-34 ($p < 0.05$). Fusion in the groups treated with 0 or 50 μg of rhBMP-2 did not change significantly with the administration of PTH 1-34 (in both groups treated with 0 μg of rhBMP-2, fusion occurred in zero of eight [0%] spines regardless of whether PTH 1-34 was used; in the groups treated with 50 μg of rhBMP-2, fusion increased from seven of eight [88%] to eight of eight [100%] with the use of PTH 1-34) (Table I).

Manual Assessment

All the spines in Groups E and F, which were treated with 50 μg of rhBMP-2, were assessed with manual palpation and were considered to have fused (eight of eight in each group, 100%). None of the spines in Groups A or B, which were treated with 0 μg of rhBMP-2, were considered to have fused (zero of eight in each group, 0%). Fusion in the spines that were treated with

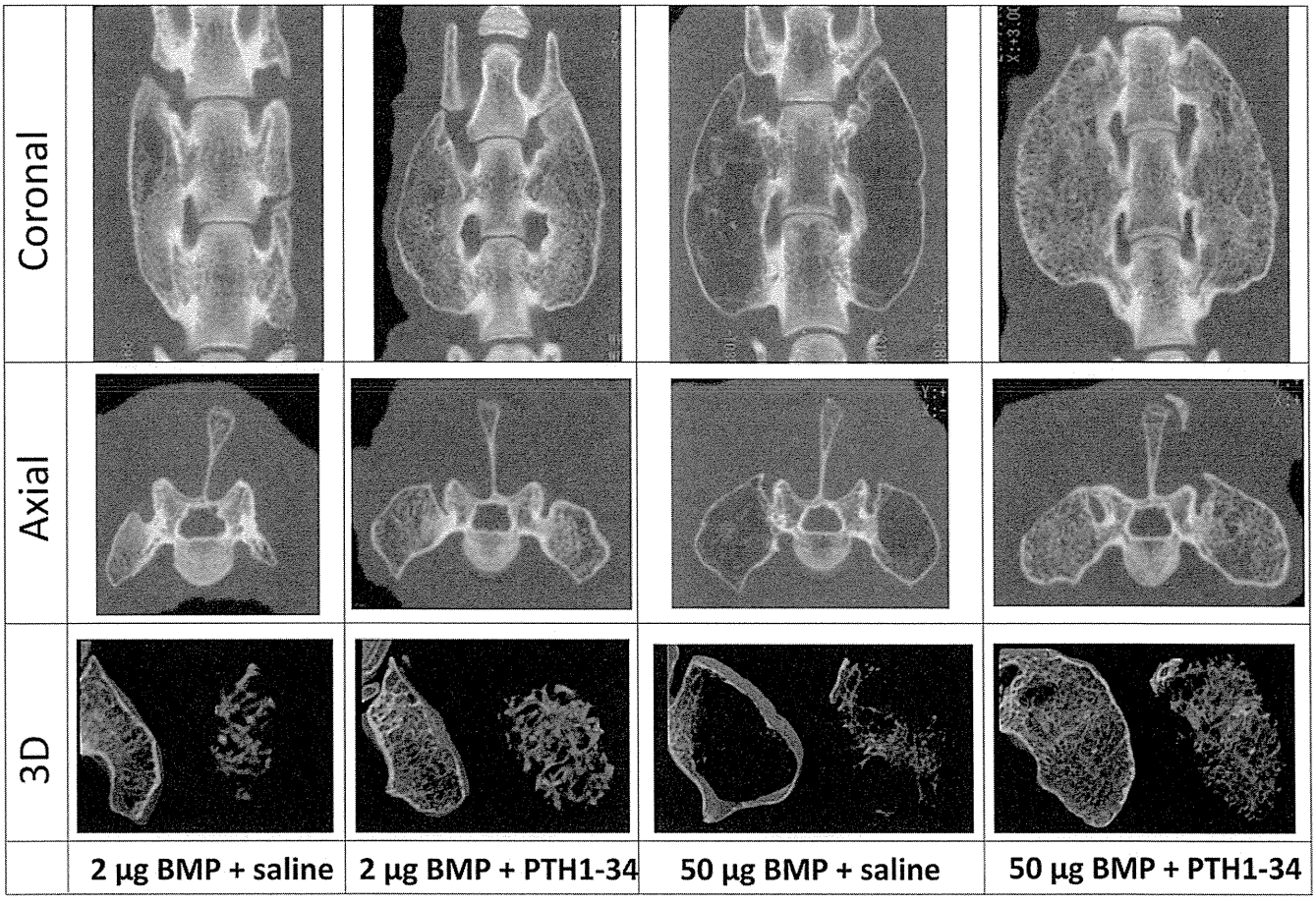

Fig. 1

In the groups treated with 2 μg of recombinant human bone morphogenetic protein (BMP)-2, the administration of teriparatide (parathyroid hormone [PTH] 1-34) improved osseous bridging between the transverse processes, the volume of the fusion mass, and the trabecular bone volume inside the fusion mass. In the group treated with 50 μg of rhBMP-2 and saline solution, the induced fusion mass resembled an eggshell (a thin outer layer of cortical bone with scarce trabecular bone inside). PTH 1-34 administration with 50-μg rhBMP-2 treatment resulted in the formation of a fusion mass that was completely filled with thick trabecular bone. 3D = three-dimensional.

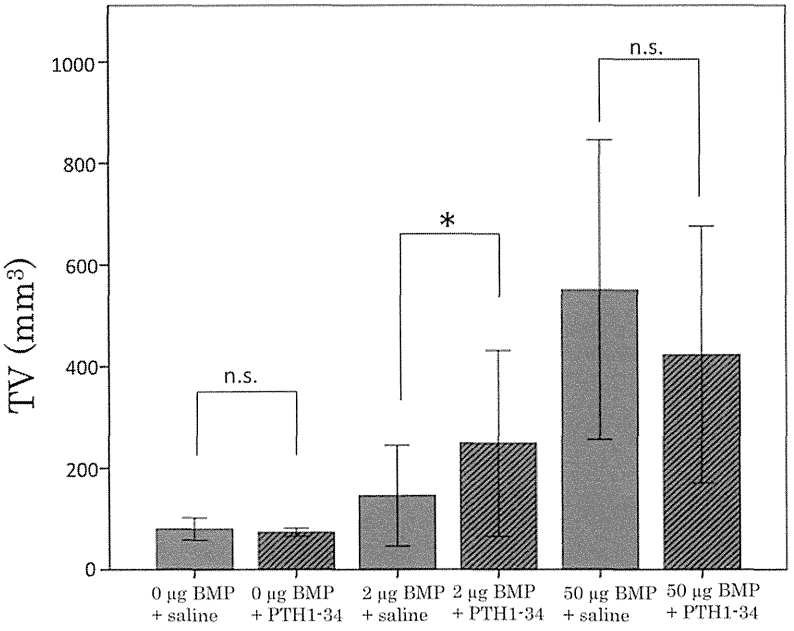

Fig. 2
Teriparatide (parathyroid hormone [PTH] 1-34) administration did not change the tissue volume (TV) in the 0-μg bone morphogenetic protein (BMP) groups. In the groups treated with 2 μg of rhBMP-2, PTH 1-34 administration significantly increased the tissue volume (TV) ($p < 0.05$). In the 50-μg rhBMP-2 groups, PTH 1-34 administration showed a decreasing trend; however, it was not significant (n.s.). The asterisk indicates a significant difference in tissue volume.

2 μg of rhBMP-2 increased from two of seven (29%, Group C) to eight of eight (100%, Group D) with the administration of PTH 1-34 ($p < 0.01$) (Table II).

Micro-CT Analysis

Analysis of the Microstructural Indices of the Fused Spinal Segments

The specimens treated with 2 or 50 μg of rhBMP-2 (Groups C, D, E, and F) were used for this analysis, because the specimens treated with 0 μg of rhBMP-2 (Groups A and B) showed little or no new bone formation.

The trabecular bone volume and structural parameters (bone volume, bone volume density, and trabecular thickness) in the groups treated with 2 μg or 50 μg of rhBMP-2 were significantly increased with the administration of PTH 1-34, and the trabecular number in the group treated with 50 μg of rhBMP-2 was also significantly increased with PTH 1-34 administration ($p < 0.01$). The cortical bone parameters of the groups treated with 2 μg or 50 μg of rhBMP-2 were also increased with the administration of PTH 1-34. Interestingly, the tissue volume in the group treated with 50 μg of rhBMP-2 decreased with the use of PTH 1-34, although the tissue volume in the groups treated with 2 μg of rhBMP-2 was significantly increased with the use of PTH 1-34 (Table III). Micro-CT coronal and axial two-dimensional images and reconstructed three-dimensional images of the newly formed bone clearly demonstrated abundant trabecular bone formation in the groups treated with PTH 1-34 (Fig. 1).

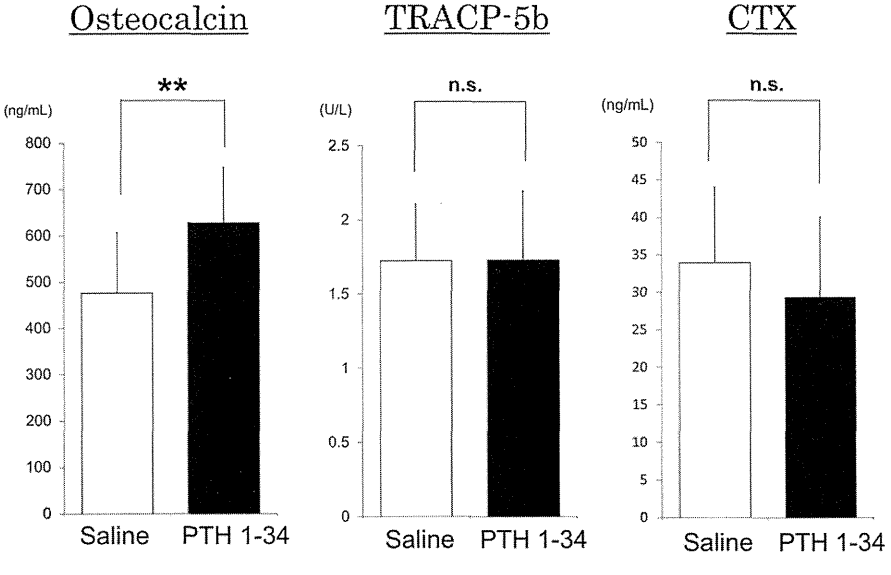

Fig. 3
Osteocalcin (bone-formation marker) levels were significantly increased with the administration of teriparatide (parathyroid hormone [PTH] 1-34) ($p < 0.01$), but tartrate-resistant acid phosphatase (TRACP)-5b (bone-resorption marker) and type-I collagen cross-linked C-telopeptides (CTX) (bone-resorption marker) levels were not significantly altered (n.s.). The double asterisk indicates a significant difference in tissue volume.

Microstructural Analysis of the Fused Spinal Segments

The mean bone volume density (and standard deviation) in Groups A and B, which received 0 μg, was 18.5% ± 3.5% and 27.8% ± 7.4% ($p < 0.01$), respectively. In Groups C and D, which received 2 μg, it was 19.6% ± 3.4% and 23.4% ± 4.8% ($p < 0.05$), respectively. In Groups E and F, which received 50 μg, it was 13.7% ± 4.2% and 24.2% ± 6.0% ($p < 0.01$), respectively. However, the alterations in tissue volume values caused by PTH 1-34 use differed in each group. The tissue volume between the groups treated with 0 μg of rhBMP-2 with or without PTH 1-34 did not differ significantly (Group A, 79.8 ± 10.2 mm^3; Group B, 72.4 ± 5.1 mm^3; $p = 0.14$). The tissue volume in the groups treated with 2 μg of rhBMP-2 significantly increased with the use of PTH 1-34 (Group C, 145.4 ± 49.6 mm^3; Group D, 239.1 ± 88.6 mm^3; $p < 0.05$); the tissue volume in the groups treated with 50 μg of rhBMP-2 decreased with the use of PTH 1-34, although the change was not significant (Group E, 469.1 ± 207.0 mm^3; Group F, 397.3 ± 137.8 mm^3; $p = 0.44$) (Fig. 2). The effect of PTH 1-34 use on tissue volume was anabolic in the 2-μg BMP group and was catabolic in the 50-μg BMP group.

Analysis of the Effect of PTH Administration on the Adjacent Vertebra (L6) and Femur

The bone volume densities of both the distal femoral epiphysis and the L6 vertebral body were significantly increased with the use of PTH 1-34 compared with those treated without PTH 1-34 (femur: 18.5% ± 10.3% compared with 49.4% ± 14.1%, $p < 0.001$; L6 vertebra: 26.1% ± 10.4% compared with 37.7% ± 4.2%, $p < 0.001$). The bone volume density of both the femur and the L6 vertebra did not differ based on the dosage of rhBMP-2.

Analysis of Serum Markers of Bone Metabolism

Enzyme-linked immunosorbent assay demonstrated that serum levels of osteocalcin were significantly higher in the groups treated with PTH 1-34 compared with those treated with saline solution ($p < 0.01$), whereas no differences were observed in serum levels of type-I collagen cross-linked C-telopeptides and tartrate-resistant acid phosphatase-5b between the groups treated with saline solution and those treated with PTH 1-34 (Fig. 3).

Histologic Analysis

Microscopic evaluation of the coronal sections of the treated spinal segments demonstrated that the groups treated with 0 μg of rhBMP-2 (Groups A and B) showed minimal evidence of new bone, and no apparent difference was noted with regard to PTH 1-34 administration (Figs. 4-A and 4-B). In the Group C rats treated with 2 μg of rhBMP-2 and injections of saline solution, the fusion mass between the L4-L5 transverse processes was discontinuous or separated by cartilage tissue (Fig. 4-C). However, in the group with the same 2-μg rhBMP-2 dosage (Group D), the addition of PTH 1-34 clearly improved the osseous continuity between the transverse processes and increased the volume of the fusion mass (Fig. 4-D). In the groups treated with 50 μg of rhBMP-2, a huge fusion mass was found even in the group that received saline solution injections (Group E); however, a majority of the newly formed fusion masses in Group E comprised fatty marrow within thin, eggshell-like cortical bone (Fig. 4-E). PTH 1-34 markedly increased the number and thickness of trabecular bone in the fusion mass (Fig. 4-F).

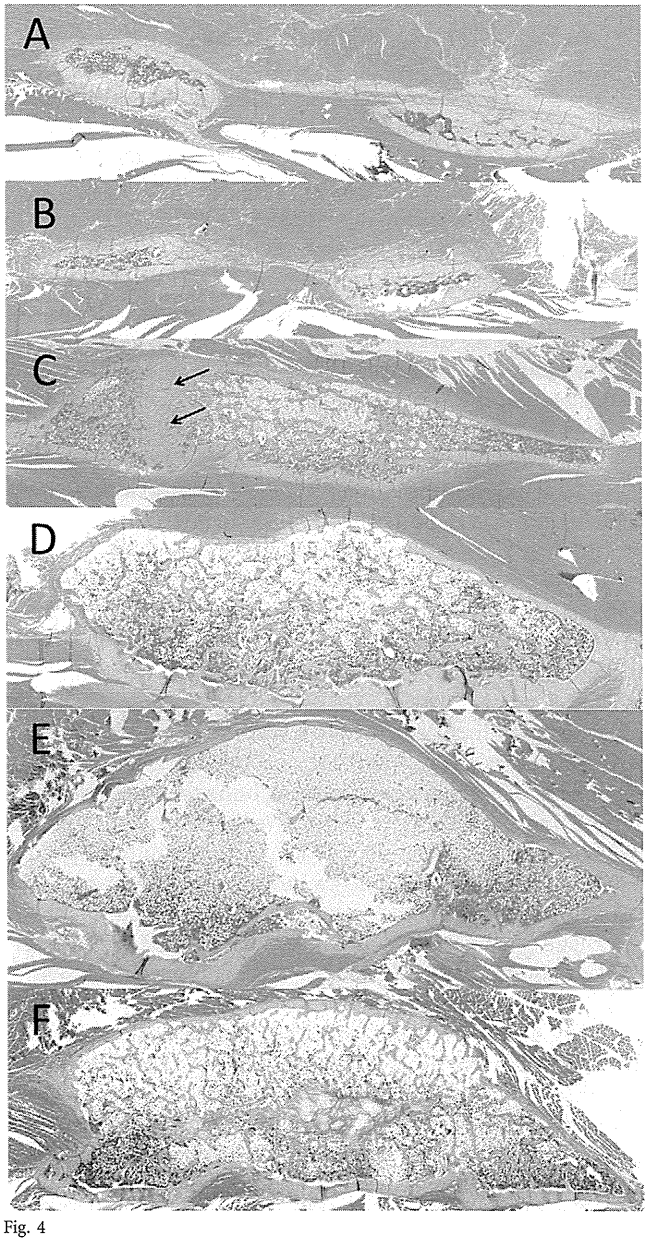

Fig. 4

Low-power photomicrographs (magnification, ×0.5). Coronal sections of the L4-L5 transverse processes of the spines of rats from Group A (Fig. 4-A) and Group B (Fig. 4-B) demonstrate no evidence of bone formation between the transverse processes. Cross-section of the transverse processes of rats from Group C (Fig. 4-C) show fibrocartilaginous union (arrows). In Group D, PTH 1-34 administration clearly improved the osseous continuity and the bone volume of the fusion mass (Fig. 4-D). In Group E (50 μg of rhBMP-2), a huge fusion mass was found; however, the fusion mass comprised fatty marrow within thin, eggshell-like cortical bone (Fig. 4-E). In Group F, PTH 1-34 administration markedly increased the number and thickness of trabecular bone in the fusion mass (Fig. 4-F).

Discussion

Intermittent PTH 1-34 administration significantly increased fusion rates in the low-dose rhBMP-2 treatment group and improved the quality of the newly formed bone in both the low-dose and the high-dose rhBMP-2 groups in a rat model of spinal fusion. The amount in the low-dose rhBMP-2 group (2 μg) is approximately one-fifth of the amount that has been commonly used in previous studies[17,19]. This reduction in dosage facilitates a decrease in the therapeutic dose of rhBMP-2, which can consequently result in a decrease in the adverse effects associated with the uncontrolled release of high-dose rhBMP-2[7,8]. As we did not observe any apparent effect of PTH 1-34 on bone induction when rhBMP-2 was not administered, we believe that rhBMP-2 and PTH 1-34 have a synergistic effect on the volume and quality of the newly formed bone.

PTH 1-34 has a unique mechanism of action in bone; the continuous administration of PTH 1-34 leads to a decrease in bone volume (a catabolic effect), and the intermittent administration of PTH 1-34 leads to the formation of increased amounts of trabecular bone (an anabolic effect)[10-14]. The use of systemic PTH 1-34 therapy has been approved for the treatment of severe osteoporosis. This anabolic effect of PTH 1-34 also provides a rationale for its potential use in the treatment of other skeletal disorders. Recent studies have demonstrated that PTH 1-34 treatment enhances fracture-healing[20,21]. The results of these studies suggest that the anabolic effect of PTH 1-34 is markedly greater in newly forming bone than in bone that is undergoing normal remodeling. We hypothesized that this strong anabolic effect in newly formed bone can be applied to the bone formation that is newly induced by rhBMP-2, and the results of the present study support our hypothesis.

The precise mechanisms through which intermittent PTH administration results in bone formation remain elusive[22-25]. PTH in vitro enhances the differentiation of mesenchymal stem cells into the osteoblast lineage[12]; however, the traditional signaling pathway of PTH does not appear to satisfactorily account for these anabolic effects. Modification of the extracellular BMP antagonist network via the low-density lipoprotein receptor-related protein 6 (LRP6), which functions in the canonical Wnt pathway and forms a complex with both PTH type-1 receptor (PTH1R) and BMP antagonists, was recently identified as one of the mechanisms through which PTH influences the differentiation of mesenchymal stem cells into the osteoblast lineage[15]. PTH stimulates the endocytosis of the PTH1R/LRP6/BMP antagonist complex, thus facilitating the enhancement of BMP signaling by blocking the negative-feedback mechanism of BMP antagonists, including noggin[15]. Another synergism between rhBMP-2 and PTH is typically seen in the groups receiving 50 μg of rhBMP-2. A high dose of rhBMP-2 is reported to induce formation of cyst-like bone voids filled with adipose tissue instead of with normal trabecular bone structure despite complete bone union[26]. Pleiotropic effects (osteoblastogenesis, adipogenesis, and osteoclastogenesis) of BMPs are mainly controlled by the BMP signaling pathway and the canonical Wnt pathway[8,9,27]. Excessive BMP signaling upregulates the expression of *Sost*, leading to the increased translation of sclerostin, which negatively regulates the Wnt pathway[16]. Downregulation of the Wnt pathway results in activation of the transcription of peroxisome proliferator-activated receptor gamma (PPARγ). This activation of PPARγ, which is a key regulator of adipocyte commitment[27], leads mesenchymal stem cells to differentiate into adipocytes rather than into osteoblasts. The activation of the Wnt pathway by PTH can downregulate PPARγ expression and promote osteoblastogenesis by BMPs.

These data suggest that the concomitant administration of PTH 1-34 and rhBMP-2 could be an ideal combination for inducing new bone formation, as PTH can induce a synergistic anabolic effect by accelerating the osteoblastic differentiation of the rhBMP-2-induced mesenchymal progenitor cells and can attenuate the negative-feedback mechanism by blocking the action of BMP antagonists.

Although PTH 1-34 injections were initiated on the day of surgery or a few days after surgery in many previous studies[28-32], our injections were initiated two weeks prior to surgery. This earlier treatment with PTH 1-34 was performed to maximize its effect on rhBMP-2, as PTH 1-34 requires approximately two weeks to exert its anabolic effect on bone metabolism, and rhBMP-2 can only persist locally for a few days after implantation.

The systemic effect of PTH 1-34 was confirmed with the increase in the bone volume density at the adjacent vertebra (L6) and femur.

PTH 1-34 administration is expected to accelerate the remodeling of newly formed bone because PTH 1-34 enhances both osteogenic and osteoclastic activity. In fact, the excessively induced new bone in the 50-μg rhBMP-2 treatment groups showed a decreasing trend in tissue volume at six weeks after surgery, which appeared to be caused by PTH 1-34 administration. Thus, PTH 1-34 may promote the remodeling process of rhBMP-2-induced newly formed bone, depending on the mechanical requirements[33].

The current results of a spinal fusion model with quadrupedal rodents cannot be directly extrapolated to spinal arthrodesis in humans because of the differences in biomechanics and biological reaction to the agents. Another limitation is a lack of biomechanical assessment of fusion because of the size and complex geometry of the rat spine. However, the results of the manual palpation test performed in this study have been shown to correlate with those of biomechanical testing[34].

In conclusion, the present study demonstrated that intermittent PTH 1-34 administration significantly increased fusion rates in the low-dose rhBMP-2 treatment group, thus indicating the potential to reduce the required rhBMP-2 dose and improve the quality of the newly formed bone in both the low and high-dose rhBMP-2 treatment groups in a rat model of rhBMP-2-induced spinal fusion. Our results indicate that the combined administration of rhBMP-2 and PTH 1-34 has a synergistic effect rather than an additive effect. Thus, we believe that PTH 1-34 has potential clinical applications in BMP-induced spinal fusion surgery.

Appendix

(eA) A table showing the six different treatment groups and a figure demonstrating the regions of interest for

the evaluation of the newly formed bone are available with the online version of this article as a data supplement at jbjs.org. ■

Note: rhPTH 1-34 was kindly provided by Asahi Kasei (Tokyo, Japan), and rhBMP-2 was kindly provided by Osteopharma (Osaka, Japan).

Tokimitsu Morimoto, MD
Takashi Kaito, MD, PhD
Masafumi Kashii, MD, PhD
Yohei Matsuo, MD
Tsuyoshi Sugiura, MD
Motoki Iwasaki, MD
Hideki Yoshikawa, MD, PhD
Departments of Orthopedic Surgery (T.M., T.K., M.K., M.I., and H.Y.) and Orthopedic Biomaterial Science (Y.M. and T.S.),
Graduate School of Medicine,
Osaka University,
2-1 Yamadaoka, Suita,
Osaka, 565-0871 Japan.
E-mail address for T. Kaito: takashikaito@gmail.com

References

1. Arrington ED, Smith WJ, Chambers HG, Bucknell AL, Davino NA. Complications of iliac crest bone graft harvesting. Clin Orthop Relat Res. 1996 Aug;(329):300-9.

2. Robertson PA, Wray AC. Natural history of posterior iliac crest bone graft donation for spinal surgery: a prospective analysis of morbidity. Spine (Phila Pa 1976). 2001 Jul 1;26(13):1473-6.

3. Steinmann JC, Herkowitz HN. Pseudarthrosis of the spine. Clin Orthop Relat Res. 1992 Nov;(284):80-90.

4. Zdeblick TA. A prospective, randomized study of lumbar fusion. Preliminary results. Spine (Phila Pa 1976). 1993 Jun 15;18(8):983-91.

5. Wozney JM, Rosen V, Celeste AJ, Mitsock LM, Whitters MJ, Kriz RW, Hewick RM, Wang EA. Novel regulators of bone formation: molecular clones and activities. Science. 1988 Dec 16;242(4885):1528-34.

6. Wang EA, Rosen V, D'Alessandro JS, Bauduy M, Cordes P, Harada T, Israel DI, Hewick RM, Kerns KM, LaPan P, et al. Recombinant human bone morphogenetic protein induces bone formation. Proc Natl Acad Sci U S A. 1990 Mar;87(6):2220-4.

7. Urist MR. Bone: formation by autoinduction. Science. 1965 Nov 12;150(3698):893-9.

8. Shields LB, Raque GH, Glassman SD, Campbell M, Vitaz T, Harpring J, Shields CB. Adverse effects associated with high-dose recombinant human bone morphogenetic protein-2 use in anterior cervical spine fusion. Spine (Phila Pa 1976). 2006 Mar 1;31(5):542-7.

9. Smucker JD, Rhee JM, Singh K, Yoon ST, Heller JG. Increased swelling complications associated with off-label usage of rhBMP-2 in the anterior cervical spine. Spine (Phila Pa 1976). 2006 Nov 15;31(24):2813-9.

10. Dempster DW, Cosman F, Parisien M, Shen V, Lindsay R. Anabolic actions of parathyroid hormone on bone. Endocr Rev. 1993 Dec;14(6):690-709.

11. Jilka RL. Molecular and cellular mechanisms of the anabolic effect of intermittent PTH. Bone. 2007 Jun;40(6):1434-46. Epub 2007 Apr 06.

12. Tam CS, Heersche JN, Murray TM, Parsons JA. Parathyroid hormone stimulates the bone apposition rate independently of its resorptive action: differential effects of intermittent and continuous administration. Endocrinology. 1982 Feb;110(2):506-12.

13. Canalis E. Update in new anabolic therapies for osteoporosis. J Clin Endocrinol Metab. 2010 Apr;95(4):1496-504.

14. Canalis E, Giustina A, Bilezikian JP. Mechanisms of anabolic therapies for osteoporosis. N Engl J Med. 2007 Aug 30;357(9):905-16.

15. Yu B, Zhao X, Yang C, Crane J, Xian L, Lu W, Wan M, Cao X. Parathyroid hormone induces differentiation of mesenchymal stromal/stem cells by enhancing bone morphogenetic protein signaling. J Bone Miner Res. 2012 Sep;27(9):2001-14.

16. Kamiya N, Ye L, Kobayashi T, Mochida Y, Yamauchi M, Kronenberg HM, Feng JQ, Mishina Y. BMP signaling negatively regulates bone mass through sclerostin by inhibiting the canonical Wnt pathway. Development. 2008 Nov;135(22):3801-11. Epub 2008 Oct 16.

17. Wang JC, Kanim LE, Yoo S, Campbell PA, Berk AJ, Lieberman JR. Effect of regional gene therapy with bone morphogenetic protein-2-producing bone marrow cells on spinal fusion in rats. J Bone Joint Surg Am. 2003 May;85(5):905-11.

18. Abe Y, Takahata M, Ito M, Irie K, Abumi K, Minami A. Enhancement of graft bone healing by intermittent administration of human parathyroid hormone (1-34) in a rat spinal arthrodesis model. Bone. 2007 Nov;41(5):775-85. Epub 2007 Jul 13.

19. Miyazaki M, Morishita Y, He W, Hu M, Sintuu C, Hymanson HJ, Falakassa J, Tsumura H, Wang JC. A porcine collagen-derived matrix as a carrier for recombinant human bone morphogenetic protein-2 enhances spinal fusion in rats. Spine J. 2009 Jan-Feb;9(1):22-30. Epub 2008 Sep 19.

20. Hernández A, Reyes R, Sánchez E, Rodríguez-Évora M, Delgado A, Évora C. In vivo osteogenic response to different ratios of BMP-2 and VEGF released from a biodegradable porous system. J Biomed Mater Res A. 2012 Sep;100(9):2382-91. Epub 2012 Apr 24.

21. Neer RM, Arnaud CD, Zanchetta JR, Prince R, Gaich GA, Reginster JY, Hodsman AB, Eriksen EF, Ish-Shalom S, Genant HK, Wang O, Mitlak BH. Effect of parathyroid hormone (1-34) on fractures and bone mineral density in postmenopausal women with osteoporosis. N Engl J Med. 2001 May 10;344(19):1434-41.

22. Seebach C, Skripitz R, Andreassen TT, Aspenberg P. Intermittent parathyroid hormone (1-34) enhances mechanical strength and density of new bone after distraction osteogenesis in rats. J Orthop Res. 2004 May;22(3):472-8.

23. Nakao Y, Koike T, Ohta Y, Manaka T, Imai Y, Takaoka K. Parathyroid hormone enhances bone morphogenetic protein activity by increasing intracellular 3′, 5′-cyclic adenosine monophosphate accumulation in osteoblastic MC3T3-E1 cells. Bone. 2009 May;44(5):872-7. Epub 2009 Jan 31.

24. Takase H, Yano S, Yamaguchi T, Kanazawa I, Hayashi K, Yamamoto M, Yamauchi M, Sugimoto T. Parathyroid hormone upregulates BMP-2 mRNA expression through mevalonate kinase and Rho kinase inhibition in osteoblastic MC3T3-E1 cells. Horm Metab Res. 2009 Dec;41(12):861-5. Epub 2009 Aug 11.

25. Jüppner H, Abou-Samra AB, Freeman M, Kong XF, Schipani E, Richards J, Kolakowski LF Jr, Hock J, Potts JT Jr, Kronenberg HM, et al. A G protein-linked receptor for parathyroid hormone and parathyroid hormone-related peptide. Science. 1991 Nov 15;254(5034):1024-6.

26. Zara JN, Siu RK, Zhang X, Shen J, Ngo R, Lee M, Li W, Chiang M, Chung J, Kwak J, Wu BM, Ting K, Soo C. High doses of bone morphogenetic protein 2 induce structurally abnormal bone and inflammation in vivo. Tissue Eng Part A. 2011 May;17(9-10):1389-99. Epub 2011 Mar 03.

27. Takada I, Kouzmenko AP, Kato S. Wnt and PPARgamma signaling in osteoblastogenesis and adipogenesis. Nat Rev Rheumatol. 2009 Aug;5(8):442-7. Epub 2009 Jul 07.

28. Kempen DH, Lu L, Hefferan TE, Creemers LB, Heijink A, Maran A, Dhert WJ, Yaszemski MJ. Enhanced bone morphogenetic protein-2-induced ectopic and orthotopic bone formation by intermittent parathyroid hormone (1-34) administration. Tissue Eng Part A. 2010 Dec;16(12):3769-77. Epub 2010 Sep 09.

29. Morgan EF, Mason ZD, Bishop G, Davis AD, Wigner NA, Gerstenfeld LC, Einhorn TA. Combined effects of recombinant human BMP-7 (rhBMP-7) and parathyroid hormone (1-34) in metaphyseal bone healing. Bone. 2008 Dec;43(6):1031-8. Epub 2008 Aug 09.

30. Tsiridis E, Morgan EF, Bancroft JM, Song M, Kain M, Gerstenfeld L, Einhorn TA, Bouxsein ML, Tornetta P 3rd. Effects of OP-1 and PTH in a new experimental model for the study of metaphyseal bone healing. J Orthop Res. 2007 Sep;25(9):1193-203.

31. Ming N, Cheng JT, Rui YF, Chan KM, Kuhstoss S, Ma YL, Sato M, Wang Y, Li G. Dose-dependent enhancement of spinal fusion in rats with teriparatide (PTH[1-34]). Spine (Phila Pa 1976). 2012 Jul 1;37(15):1275-82.

32. Drake MT, Srinivasan B, Mödder UI, Ng AC, Undale AH, Roforth MM, Peterson JM, McCready LK, Riggs BL, Khosla S. Effects of intermittent parathyroid hormone treatment on osteoprogenitor cells in postmenopausal women. Bone. 2011 Sep;49(3):349-55. Epub 2011 May 11.

33. Komatsubara S, Mori S, Mashiba T, Nonaka K, Seki A, Akiyama T, Miyamoto K, Cao Y, Manabe T, Norimatsu H. Human parathyroid hormone (1-34) accelerates the fracture healing process of woven to lamellar bone replacement and new cortical shell formation in rat femora. Bone. 2005 Apr;36(4):678-87.

34. Boden SD, Schimandle JH, Hutton WC. An experimental lumbar intertransverse process spinal fusion model. Radiographic, histologic, and biomechanical healing characteristics. Spine (Phila Pa 1976). 1995 Feb 15;20(4):412-20.

J Bone Miner Metab (2014) 32:378–392
DOI 10.1007/s00774-013-0514-1

ORIGINAL ARTICLE

IL-6 negatively regulates osteoblast differentiation through the SHP2/MEK2 and SHP2/Akt2 pathways in vitro

Shoichi Kaneshiro · Kosuke Ebina · Kenrin Shi · Chikahisa Higuchi · Makoto Hirao · Michio Okamoto · Kota Koizumi · Tokimitsu Morimoto · Hideki Yoshikawa · Jun Hashimoto

Received: 13 February 2013 / Accepted: 7 August 2013 / Published online: 12 October 2013

Abstract It has been suggested that interleukin-6 (IL-6) plays a key role in the pathogenesis of rheumatoid arthritis (RA), including osteoporosis not only in inflamed joints but also in the whole body. However, previous in vitro studies regarding the effects of IL-6 on osteoblast differentiation are inconsistent. The aim of this study was to examine the effects and signal transduction of IL-6 on osteoblast differentiation in MC3T3-E1 cells and primary murine calvarial osteoblasts. IL-6 and its soluble receptor significantly reduced alkaline phosphatase (ALP) activity, the expression of osteoblastic genes (Runx2, osterix, and osteocalcin), and mineralization in a dose-dependent manner, which indicates negative effects of IL-6 on osteoblast differentiation. Signal transduction studies demonstrated that IL-6 activated not only two major signaling pathways, SHP2/MEK/ERK and JAK/STAT3, but also the SHP2/PI3K/Akt2 signaling pathway. The negative effect of IL-6 on osteoblast differentiation was restored by inhibition of MEK as well as PI3K, while it was enhanced by inhibition of STAT3. Knockdown of MEK2 and Akt2 transfected with siRNA enhanced ALP activity and gene expression of Runx2. These results indicate that IL-6 negatively regulates osteoblast differentiation through SHP2/MEK2/ERK and SHP2/PI3K/Akt2 pathways, while affecting it positively through JAK/STAT3. Inhibition of MEK2 and Akt2 signaling in osteoblasts might be of potential use in the treatment of osteoporosis in RA.

Keywords Interleukin-6 · Osteoblast differentiation · MEK2 · Akt2 · Signaling pathway

Introduction

Inflammation-mediated bone loss is a major feature of various bone diseases, including rheumatoid arthritis (RA). Interleukin-6 (IL-6) contributes to the development of arthritis and is present at high concentrations in the serum and synovial fluid of patients with RA [1–4]. Soluble IL-6 receptor (sIL-6R) is also elevated in the serum and synovial fluid of RA patients [5, 6], and IL-6 exerts its action by binding either to its membrane-bound receptor (mIL-6R) or to sIL-6R. Moreover, IL-6 is closely associated with the expression of receptor activator of NF-κB ligand (RANKL) in osteoblasts [7]. That is to say, IL-6 acts indirectly on osteoclastogenesis by stimulating the release of RANKL by cells within bone tissues such as osteoblasts [8]. It can unquestionably be said that IL-6 plays a major role in the pathogenesis of RA [9–12], including osteoporosis not only in inflamed joints but also in the whole body.

There have been several studies on the effect of IL-6 on bone turnover in animal models. In IL-6 knock-out mice,

Electronic supplementary material The online version of this article (doi:10.1007/s00774-013-0514-1) contains supplementary material, which is available to authorized users.

S. Kaneshiro · K. Ebina (✉) · K. Shi · C. Higuchi · M. Okamoto · K. Koizumi · T. Morimoto · H. Yoshikawa
Department of Orthopaedic Surgery, Graduate School of Medicine, Osaka University, 2-2 Yamadaoka, Suita, Osaka 565-0871, Japan
e-mail: k-ebina@umin.ac.jp

M. Hirao
Department of Orthopaedic Surgery, Osaka Minami Medical Center, National Hospital Organization, 2-1 Kidohigashi, Kawachinagano, Osaka 586-8521, Japan

J. Hashimoto
Department of Rheumatology, Osaka Minami Medical Center, National Hospital Organization, 2-1 Kidohigashi, Kawachinagano, Osaka 586-8521, Japan

microstructure abnormalities in cortical bones and delayed fracture healing were observed [13, 14], in spite of the evident normal phenotype [15]. Also, bone loss after estrogen depletion was mitigated in IL-6-deficient mice, while a high level of IL-6 and bone loss are seen in wild-type mice [13]. Moreover, IL-6-overexpressed-transgenic mice develop osteopenia and defective ossification, in which the activity of mature osteoblasts is significantly decreased [16]. All these findings, together with studies on human RA patients [17, 18], indicate that IL-6 plays a major role in bone turnover and is an important regulator of bone homeostasis.

Recently, several biological agents have been introduced for the treatment of RA and have demonstrated not only potent anti-inflammatory effects but also inhibitory effects on joint destruction. Among these biological agents, tocilizumab, an anti-IL-6 receptor antibody, has been reported to increase serum bone formation markers in RA patients [19], suggesting that IL-6 has a negative effect on osteoblast differentiation. However, previous reports regarding the effects of IL-6 on osteoblast differentiation in vitro have been inconsistent [20]. IL-6 has been shown to decrease the expression of differentiation markers in osteoblasts [21, 22] and to inhibit bone formation [23], while it has been shown to induce osteoblast differentiation [24, 25].

Binding of IL-6 with sIL-6R or mIL-6R leads to subsequent homodimerization of the signal-transducing molecule gp130, followed by activation of two major intracellular signaling pathways, Janus protein tyrosine kinase (JAK)/signal transducer and activator of transcription factors (STAT) 3, or Src-homology domain 2 containing protein-tyrosine phosphatase (SHP2)/mitogen-activated protein kinase-extracellular signal–regulated kinase kinase (MEK)/mitogen-activated protein kinase (MAPK), also called extracellular signal-regulated kinase (ERK) [26]. There have been many reports in which the effects of IL-6 on JAK/STAT3 and SHP2/ERK signal transduction pathways have been studied in osteoblasts, though it is still controversial whether differentiation is enhanced by IL-6 [9, 20]. SHP2 can also form a tertiary complex with the scaffolding proteins Gab1/2 and the p85 subunit of phosphatidylinositol-3-kinase (PI3K) [27], which leads to activation of the Akt pathway. Several papers have so far reported that the PI3K/Akt pathway triggered by IL-6 plays important roles in various cells [28–32], but no reports have been published regarding the effect of IL-6 on this pathway in osteoblasts.

The purpose of this study was to clarify the effect of IL-6 on osteoblast differentiation in vitro, with consideration of intracellular signaling pathways in murine MC3T3-E1 osteoblastic cells and primary murine calvarial osteoblasts.

Materials and methods

Ethics statement

Prior to the study, all experimental protocols were approved by the Ethics Review Committee for Animal Experimentation of Osaka University School of Medicine.

Cell culture

MC3T3-E1 osteoblastic cells were purchased from Riken Cell Bank (Tsukuba, Japan). MC3T3-E1 cells were cultured in α-minimum essential medium (α-MEM) containing 10 % fetal bovine serum (FBS; Equitech-Bio, Kerrville, TX, USA) and 1 % penicillin and streptomycin at 37 °C in a humidified atmosphere of 5 % CO_2. All media were purchased from Life Technologies Japan (Tokyo, Japan). Murine primary osteoblasts were isolated from the calvariae of 3-day-old C57BL/6 mice (Charles River Laboratories Japan, Inc, Osaka, Japan) by sequential collagenase digestion as described previously [33].

MC3T3-E1 cells and murine calvarial osteoblasts were seeded at 1×10^5 cells per well in 12-well plates. After the cells reached confluence, the medium was replaced to induce osteoblast differentiation. The differentiation medium contained 10 % FBS, 10 mM β-glycerophosphate, and 50 μg/ml ascorbic acid in the absence or presence of recombinant mouse (rm) IL-6 (R&D Systems, Inc., Minneapolis, MN, USA) (10, 50 ng/mL), and rm sIL-6R (R&D Systems) (100 ng/mL). The medium and reagents were renewed every 3 days.

To study signal transduction, the following inhibitors or vehicle (DMSO) (Sigma-Aldrich, St.Louis, MO, USA) were added to culture medium at several concentrations; MEK inhibitor (U0126; 1, 2.5, 5 μM; Cell Signaling Technology, Danvers, MA, USA), STAT3 inhibitor (V Stattic; 2.5, 5 μM; Calbiochem, La Jolla, CA, USA), PI3K inhibitor (LY294002; 1, 2.5, 5 μM; Cell Signaling Technology), and SHP2 inhibitor (PHPS1; 5, 20, 40 μM; Sigma-Aldrich). These inhibitors were added 1 h before treatment with IL-6/sIL-6R. All inhibitors were maintained until the end of the culture period at the indicated concentrations.

Alkaline phosphatase (ALP) staining and activity

MC3T3-E1 cells and murine calvarial osteoblasts were treated with or without IL-6/sIL-6R and signal pathway inhibitors after the cells reached confluence and were incubated for 6 days.

For ALP staining, after fixation with 10 % formalin, cells were washed twice with phosphate-buffered saline (PBS) (pH 7.4) and incubated with ALP substrate solution,

0.1 mg/ml naphthol AS-MX (Sigma-Aldrich), and 0.6 mg/ml fast violet B salt (Sigma-Aldrich) in 0.1 M Tris–HCl (pH 8.5) for 20 min.

To measure ALP activity, cells were washed twice with PBS and lysed in Mammalian Protein Extraction Reagent (Pierce, Rockford, IL, USA) according to the manufacturer's protocol. ALP activity was assayed using *p*-nitrophenylphosphate as a substrate by an Alkaline Phosphatase Test Wako (Wako Pure Chemicals Industries, Ltd., Osaka, Japan), and the protein content was measured using the Bicinchoninic Acid Protein Assay Kit (Pierce).

Proliferation assay

MC3T3-E1 cells were cultured in 96-well plates at a concentration of 2.0×10^4 cells/cm^2 in α-MEM containing 10 % FBS. Cells were incubated for 1 day, after which the medium was treated with IL-6/sIL-6R for 3 days. Cell proliferation was assessed using the Premix WST-1 Cell Proliferation Assay System (Takara Bio, Inc., Otsu, Japan) according to the manufacturer' s instructions. We performed this assay every 24 h.

Alizarin red staining

After fixation with 10 % formalin, MC3T3-E1 cells and murine calvarial osteoblasts were washed with distilled water, and stained with alizarin red S solution (Sigma-Aldrich) (pH 6.0) for 10 min, followed by incubation in 100 mM cetylpyridinium chloride for 1 h at room temperature to dissolve and release calcium-bound alizarin red. The absorbance of the released alizarin red was then measured at 570 nm [34]. To measure the value of absorbance for alizarin red, the absorbance data were normalized by total DNA content. Total DNA was extracted using a DNeasy Blood & Tissue Kit (Qiagen, Düsseldorf, Germany).

Knockdown of MEK1, MEK2, Akt1 and Akt2 using RNA interference

MC3T3-E1 cells were transfected with small interfering RNAs (siRNA) using Lipofectamine RNAiMAX (Life Technologies Japan) according to the reverse transfection method in the manufacturer's protocol.

The siRNAs for MEK2, Akt1 and Akt2 and that for MEK1 were purchased from Cell Signaling Technology and Qiagen, respectively, with negative controls for each molecule. MC3T3-E1 cells transfected with siRNA were seeded in 24-well plates at a concentration of 1.0×10^4 cells/cm^2 for 48 h. The medium was then replaced with differentiation medium with vehicle or with 20 ng/ml IL-6 and 100 ng/ml sIL-6R and the cells were incubated for 3 days prior to use for further experiments.

Western blotting

Cells cultured in 6-well plates for 2 days were washed twice with PBS and then homogenized with 100 μl of Kaplan buffer (150 mM NaCl, 50 mM Tris–HCL pH 7.4, 1 % NP40, 10 % glycerol, and 1 tablet per 50 ml buffer of protease inhibitor cocktail and phosphatase inhibitor cocktail). The lysates were centrifuged at 13,000 rpm for 20 min at 4 °C, and the supernatants were used for electrophoresis after a protein assay using bovine serum albumin as standard. Western blotting was performed by use of the following antibodies purchased from Cell Signaling Technology, except for phosphate anti-Akt2 antibody from Enogene Biotech (New York, NY, USA): phosphate anti-STAT3 (Tyr705) (1:2000) and anti-STAT3 (1:1000); phosphate anti-Akt (Ser473) (1:2000), phosphate anti-Akt2 (Ser474) (1:1000), anti-Akt1, anti-Akt2, and anti-Akt (1:1000); phosphate anti-ERK (Thr202/Tyr204) (1:2000), anti-MEK1, anti-MEK2 and anti-ERK (1:1000); and phosphate anti-SHP2 (Tyr542) (1:1000). To control for protein loading, blots were additionally stained with anti-β actin antibody (1:1000).

Reverse transcription polymerase chain reaction (RT–PCR)

Total RNA was extracted from cells with an RNeasy Mini Kit (Qiagen), and first-strand cDNA was synthesized using SuperScript II RNase H-reverse transcriptase (Life Technologies Japan). Then PCR was performed using Ex Taq (Takara Bio) and the following primers:

Osteocalcin (forward primer 5′-CTCACTCTGCTGGCCCTG-3′; reverse primer 5′-CCGTAGATGCGTTTGTAGGC-3′);
Osterix (forward primer 5′-AGGCACAAAGAAGCCATAC-3′; reverse primer 5′-AATGAGTGAGGGAAGGGT-3′);
Runx2 (forward primer 5′-GCTTGATGACTCTAAACCTA-3′; reverse primer 5′-AAAAAGGGCCCAGTTCTGAA-3′);
GAPDH (forward primer 5′-TGAACGGGAAGCTCACTGG-3′; reverse primer 5′-TCCACCACCCTGTTGCTGTA-3′).

Quantitative real-time PCR analysis

We obtained cDNA by reverse transcription as mentioned above, and proceeded with real-time PCR using a Light Cycler system (Roche Applied Science, Basel, Switzerland). The SYBR Green assay using a Quantitect SYBR Green PCR Kit (Qiagen), in which each cDNA sample was evaluated in triplicate 20-μl reactions, was used for all

target transcripts. Expression values were normalized to GAPDH.

Statistical analysis

The results are expressed as the mean ± standard error (SE). Between-group differences were assessed using the ANOVA test. A probability value of <0.05 was considered to indicate statistical significance.

Results

IL-6/sIL-6R does not affect proliferation, but significantly reduces ALP activity and expression of osteoblastic genes in MC3T3-E1 cells

We first measured the proliferation of MC3T3-E1 cells with IL-6. Cell proliferation did not show significant difference in any culture condition (Fig. 1a).

To investigate the influence of IL-6 treatment on osteoblast differentiation, we examined ALP activity in MC3T3-E1 cells. As shown in Fig. 1b and c, IL-6/sIL-6R significantly reduced ALP activity in a dose-dependent manner. The single addition of sIL-6R did not show a significant difference as compared to the negative control with vehicle. As shown in Fig. 1d and e, gene expression of Runx2, osterix and osteocalcin was significantly downregulated by IL-6/sIL-6R in a dose-dependent manner. Again, the single addition of sIL-6R did not show significant difference as compared to the negative control with vehicle.

IL-6/sIL-6R significantly inhibits mineralization of extracellular matrix (ECM) in MC3T3-E1 cells

As shown in Fig. 2a, IL-6/sIL-6R significantly inhibited the mineralized area in a dose-dependent manner. The single addition of sIL-6R did not show a significant difference as compared to the negative control with vehicle (Fig. 2a). Quantitative analysis of mineralization by measuring the absorbance of alizarin red revealed a significant decrease by IL-6/sIL-6R in a dose-dependent manner (Fig. 2b).

IL-6/sIL-6R activates ERK, STAT3 and Akt2 signal transduction pathways in MC3T3-E1 cells

When MC3T3-E1 cells were incubated in the presence of IL-6/sIL-6R, phosphorylation of ERK, STAT3 and Akt was clearly observed at 15 min, and their activation became weaker at 30 min. When only sIL-6R was added, there was no apparent activation of ERK, STAT3, or Akt as compared to the negative control (Fig. 3a). As for Akt, the phosphorylation by IL-6/sIL-6R was recognized more strikingly as early as 5 min in a dose-dependent manner, both for whole and for Akt2 only, one of its three isoforms (Fig. 3b).

IL-6-induced activation of ERK is enhanced by blocking the STAT3 signaling pathway, and IL-6-induced ERK and Akt signaling pathways negatively regulate each other reciprocally

The SHP2 inhibitor PHPS1 [35] inhibited IL-6-induced phosphorylation of ERK and Akt to the constitutive level, but did not inhibit STAT3 (Fig. 4a and Supplementary Fig. S1a), suggesting that the downstream pathways of SHP2 are ERK and Akt, not STAT3. The STAT3 inhibitor V Stattic inhibited the phosphorylation of STAT3 but enhanced ERK significantly (Fig. 4a and Supplementary Fig. S1a), suggesting that STAT3 could negatively regulate ERK, which is consistent with previous reports [36]. The MEK/ERK inhibitor U0126 completely inhibited both constitutive and IL-6-induced phosphorylation of ERK but enhanced those of Akt. Moreover, the PI3K/Akt inhibitor LY294002 completely inhibited both constitutive and IL-6-induced phosphorylation of Akt but enhanced those of ERK (Fig. 4b and Supplementary Fig. S1b). From these findings, we concluded that IL-6-induced ERK and Akt signaling pathways, both of which are downstream of SHP2, can negatively regulate each other reciprocally.

The negative effects of IL-6 on osteoblast differentiation are restored by inhibition of MEK, PI3K and SHP2, while they are enhanced by inhibition of STAT3

To identify the intracellular signaling pathways associated with the downregulation of osteoblast differentiation, the effects of various signal transduction inhibitors, consisting of a MEK inhibitor (U0126), PI3K inhibitor (LY294002), SHP2 inhibitor (PHPS1), and STAT3 inhibitor (V Stattic), were assessed for ALP activity, the expression of osteoblastic genes (Runx2, osterix and osteocalcin), and the mineralization of ECM.

The negative effect of IL-6/sIL-6R on ALP activity was restored by treatment with either U0126, LY294002, or PHPS1 in a dose-dependent manner. On the other hand, the negative effect of IL-6/sIL-6R on ALP activity was enhanced by treatment with V Stattic (Fig. 5a). These results indicate that the SHP2-associated signal transduction molecules MEK/ERK and PI3K/Akt have a negative effect on osteoblast differentiation, whereas the JAK-associated molecule STAT3 has a positive effect.

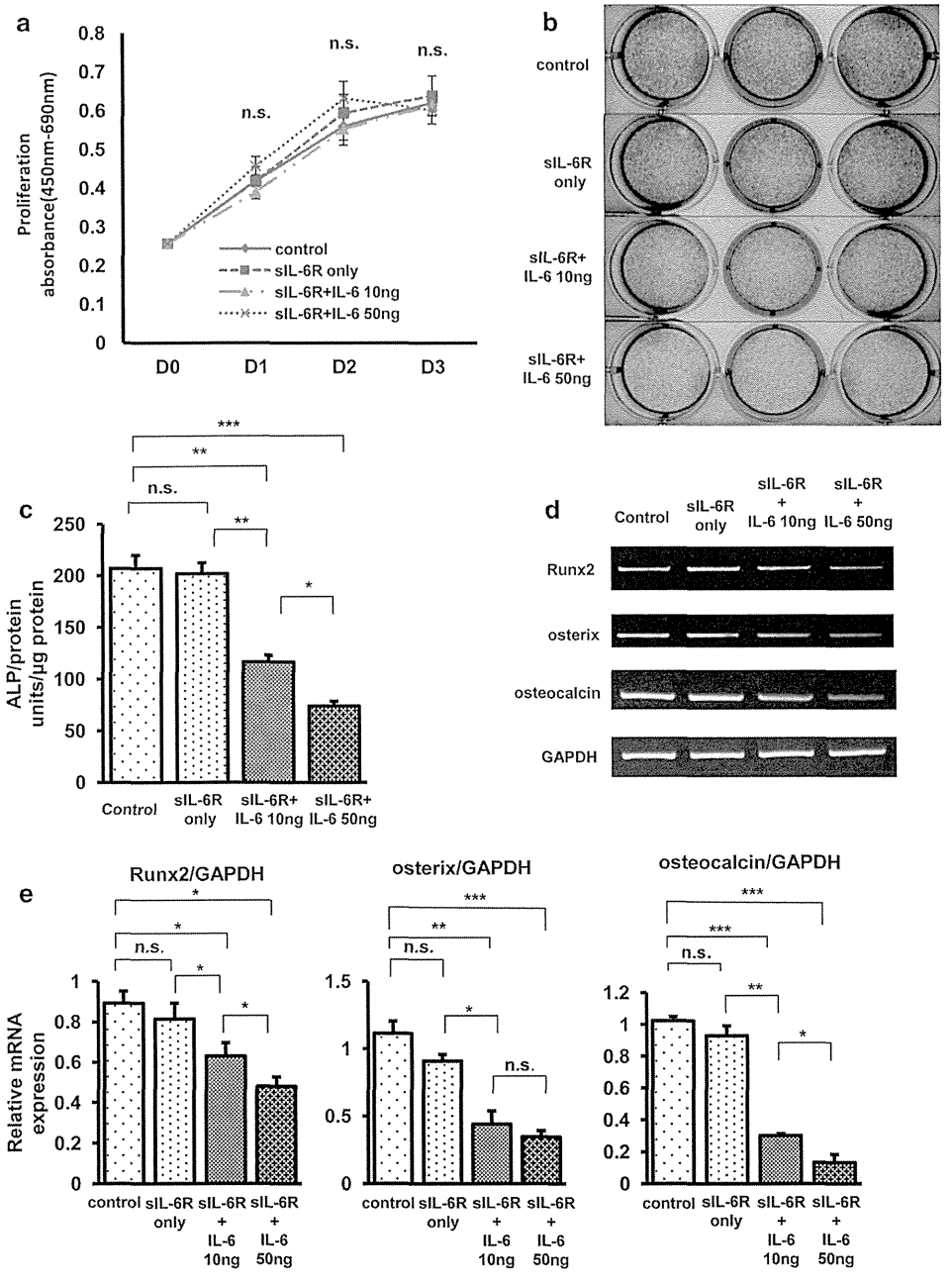

Fig. 1 IL-6/sIL-6R significantly reduced ALP activity and expression of osteoblastic genes in MC3T3E1 cells, but did not affect proliferation. **a** Proliferation of MC3T3-E1 cells with IL-6/sIL-6R was examined. Cells were pre-incubated for 1 day and then the medium was treated with or without IL-6/sIL-6R for 3 days. Cell proliferation assay was performed daily throughout the 4 days of incubation. Cell proliferation did not show significant differences in any culture condition. **b** ALP staining was performed in MC3T3-E1 cells treated with or without IL-6/sIL-6R for 6 days. Apparently significant reduction of ALP staining was recognized in cells treated with either 10 or 50 ng/ml IL-6. **c** ALP activity of the lysates of MC3T3-E1 cells treated with or without IL-6/sIL-6R for 6 days was measured using p-nitrophenylphosphate as a substrate. IL-6/sIL-6R significantly reduced ALP activity in a dose-dependent manner. **d** Total RNA was extracted from MC3T3-E1 cells treated with or without IL-6/sIL-6R for 6 days and subjected to RT-PCR for osteoblastic genes Runx2, osterix, and osteocalcin. Apparently significant reduction of osteoblastic gene expression was recognized in cells treated with either 10 or 50 ng/ml IL-6. **e** Real-time PCR for Runx2, osterix, and osteocalcin was performed for quantitative analysis. Data were normalized to GAPDH expression and are shown as the ratio of expression compared to control cells treated with vehicle. The expression of osteoblastic genes was significantly downregulated by IL-6/sIL-6R in a dose-dependent manner. Representative data from at least 3 independent experiments are shown. Data are shown as mean ± SE. *n.s.* not significant; $*P < 0.05$; $**P < 0.001$; $***P < 0.001$

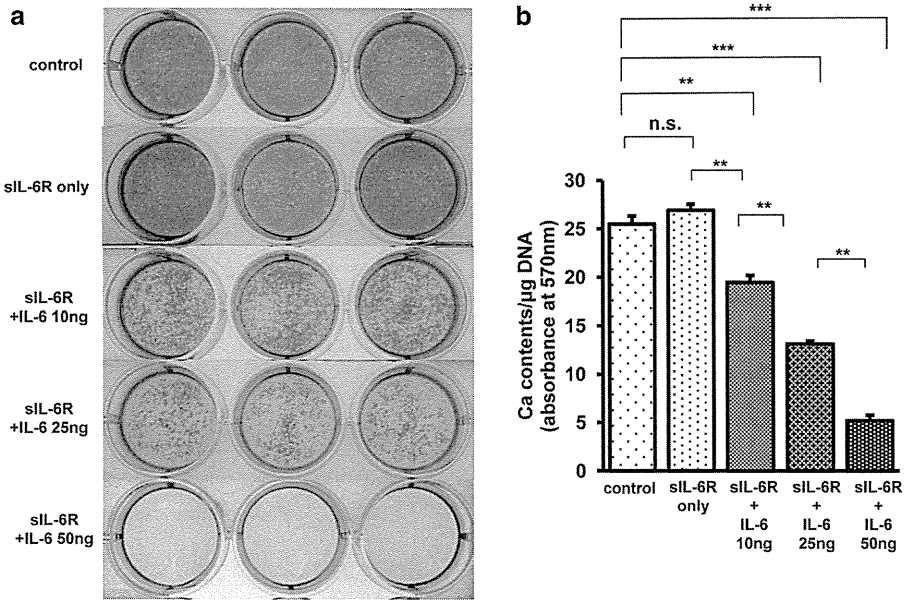

Fig. 2 IL-6/sIL-6R significantly inhibited the mineralization of ECM in MC3T3E1 cells. MC3T3-E1 cells were treated with or without IL-6/sIL-6R and were incubated for 21 days. **a** After fixation, the cells were stained with alizarin red solution. Apparently significant reduction of alizarin red staining was recognized in the cells treated with either 10, 25, or 50 ng/ml IL-6. **b** Matrix mineralization was quantified by the measurement of absorbance of alizarin red and normalized by total DNA content. Matrix mineralization was significantly reduced by IL-6/sIL-6R in a dose-dependent manner. Representative data from at least 3 independent experiments are shown. Data are shown as mean ± SE. *n.s.* not significant; $*P < 0.05$; $**P < 0.001$; $***P < 0.001$

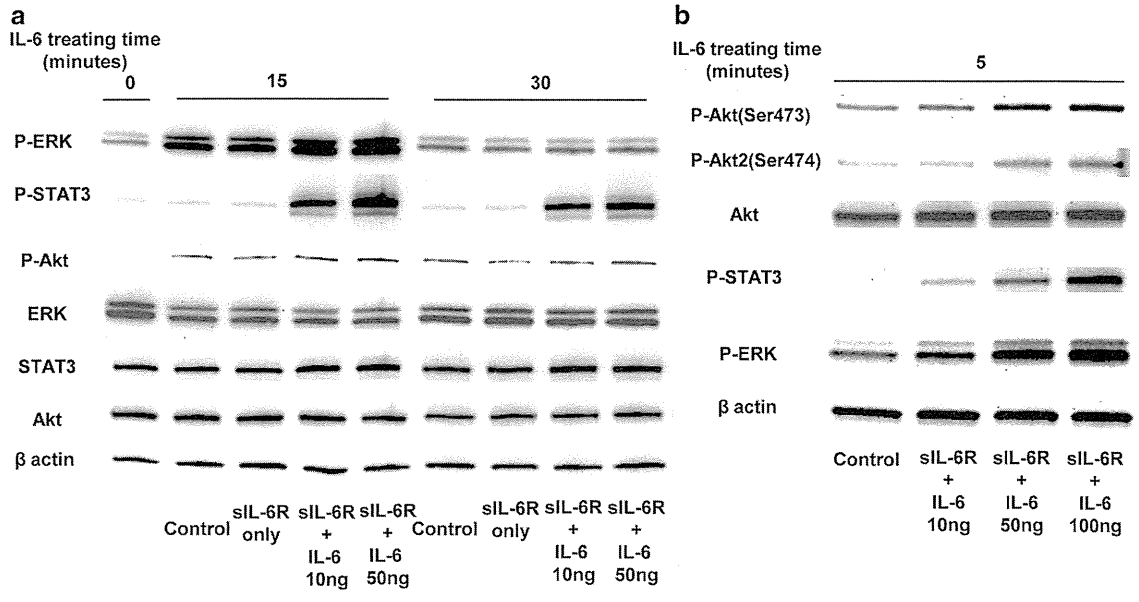

Fig. 3 IL-6/sIL-6R-activated ERK, STAT3, and Akt2 signal transduction pathways in MC3T3-E1 cells. **a** MC3T3-E1 cells were treated with vehicle or with 10 or 50 ng/ml IL-6 and 100 ng/ml sIL-6R in a time-course experiment (0, 15, and 30 min). Western blot analysis was performed using cell lysates for the detection of ERK, STAT3, and Akt, either phosphorylated or not. IL-6/sIL-6R significantly induced the phosphorylation of ERK, STAT3, and Akt in a dose-dependent manner. **b** MC3T3-E1 cells were incubated with increasing concentrations of IL-6 and 100 ng/ml sIL-6R for 5 min. Western blotting was performed using cell lysates for the detection of ERK, STAT3, as well as Akt, either non-phosphorylated, phosphorylated, or the phosphorylated isoform Akt2. The phosphorylation of both whole Akt and Akt2 by IL-6/sIL-6R was recognized more strikingly in a dose-dependent manner. Representative data from at least three independent experiments are shown